Research Square

Preprints are preliminary reports that have not undergone peer review.
They should not be considered conclusive, used to inform clinical practice,
or referenced by the media as validated information.

Geomechanically and Geochemically Constrained Natural Hydrogen Prospectivity of the Manipur Ophiolite Complex and the Indo-Burma Range, Northeast India with a National Multi-Criteria Prospectivity Ranking

DILIP KUMAR MAHATA
Indian Institute of Technology Dhanbad
SAYANTAN GHOSH
sayantan@iitism.ac.in

Indian Institute of Technology Dhanbad

Research Article

Keywords: Natural hydrogen, Geologic hydrogen, Manipur Ophiolite Complex, Indo-Burma Range, Serpentinisation, National Green Hydrogen Mission

Posted Date: November 13th, 2026

DOI: https://doi.org/10.21203/rs.3.rs-11435088/v1

License: This work is licensed under a Creative Commons Attribution 4.0 International License.
Read Full License

Additional Declarations: No competing interests reported.

Geomechanically and Geochemically Constrained Natural Hydrogen Prospectivity of the Manipur Ophiolite Complex and the Indo-Burma Range, Northeast India with a National Multi-Criteria Prospectivity Ranking

Dilip Kumar Mahata[1], Sayantan Ghosh[2*]

[1] JRF, Department of Petroleum Engineering, IIT (ISM) Dhanbad-826004, India

[2] Assistant Professor, Department of Petroleum Engineering, IIT (ISM) Dhanbad-826004, India

** Corresponding author: sayantan@iitism.ac.in*

Keywords: Natural hydrogen · Geologic hydrogen · Manipur Ophiolite Complex · Indo-Burma Range · Serpentinisation · National Green Hydrogen Mission

Abstract

Natural hydrogen (H_2) is an evolving underground energy asset, however its geological viability in India is yet inadequately defined. This research assesses ten methods for hydrogen creation and release within Indian geological regions, incorporating published petrological, geochemical, and structural data from the Manipur Ophiolite Complex (MOC) and the Indo-Burma Range. A twelve-criterion weighted prospectivity framework is enhanced by serpentinization screening, a significant hydrogen-generation estimation, and three quantitative sensitivity evaluations. Three-dimensional fault-plane traction analyses investigate Coulomb slip vulnerability under representative principal-stress conditions. A hypothesized stress–aperture closure principle assesses comparative fracture transmissivity and Monte Carlo variations also assess the responsiveness of prospectivity rankings. A geographical excerpt from the World Stress Map 2025 provides stress-orientation scenarios without serving as a direct gage of shallow MOC stress intensities. The documented ultramafic compositions and extensive serpentinization point to good source rock conditions. The overall MOC prospectivity score is 8.39 out of 10. Still, the key intra-belt goals have very similar scores, and the hydraulic properties of fractures, the effectiveness of trapping, and direct examples of subsurface hydrogen are still unknown. The proposed rankings and volumetric evaluations function as screening tools instead of confirmed accumulations or recoverable resources. Focused fluid extraction, structural assessment, and subsurface investigations are essential to validate hydrogen charge, migration and preservation.

Article Highlights

- MOC ultramafic rocks are favorable hydrogen sources, but subsurface accumulations remain unconfirmed.
- Three-dimensional fault-slip and fracture-flow calculations quantify assumption-dependent sensitivities.
- Monte Carlo tests show that the leading Manipur prospectivity rankings are not securely separated.

1. Introduction

1.1 The global natural hydrogen renaissance

Molecular hydrogen produced by geological processes is termed geologic, native, white, or gold hydrogen. It is experiencing rapidly accelerating scientific and commercial interest. The landmark discovery of a large natural H_2 accumulation at Bourakebougou, Mali (Prinzhofer et al. 2018; Maiga et al. 2023), revealed that commercially viable subsurface H_2 exists in the continental crust. It initiated a global debate on whether natural hydrogen could complement or rival green electrolytic hydrogen as a low-carbon energy carrier. Subsequent discoveries and characterisation in Oman (Kelemen et al. 2011), Turkey (Etiope & Sherwood Lollar 2013; Etiope, 2023), Newfoundland (Szponar et al. 2013), France (Lefeuvre et al. 2021), Albania (Truche et al. 2024) and elsewhere have proven that natural H_2 is neither rare nor insignificant in flux. (Milkov 2022).

Unlike green hydrogen produced by water electrolysis using renewable electricity, natural hydrogen is a product of thermodynamically spontaneous rock–water interactions, radioactive decay, or frictional processes. These processes have operated in the Earth's crust for billions of years. Its production requires no energy infrastructure, no electrolysers, and no grid connection. It is generated continuously if the relevant mineralogical and hydrological conditions are met in the subsurface. The USGS mass-balance model (Ellis & Gelman 2024) predicts a most-probable global in-place geologic H_2 resource of ~5.6×10^6 Mt. Peridotites within the upper 7 km of crust alone could generate ~10^8 Mt H_2 (Blay-Roger et al. 2024) against a 2024 global H_2 demand of ~100 Mt (International Energy Agency (IEA) 2025). The global distribution map of hydrogen in various geologic provinces is provided in **Figure 1**.

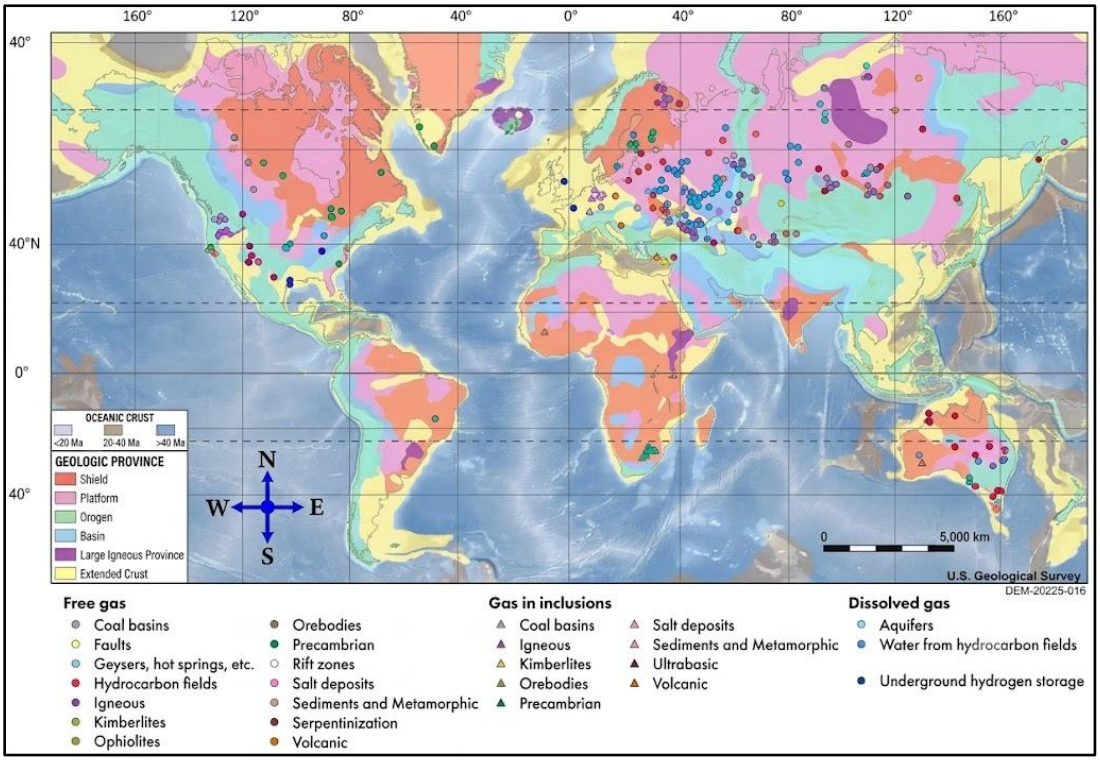


Figure 1. Global distribution of reported natural hydrogen occurrences (reproduced from Sun et al. 2025, Fig. 4, which adapts the map in Bendall 2022, Fig. 1).

1.2 India's geological diversity and H_2 opportunity

The Indian subcontinent occupies a unique position in global tectonics. These include Archean cratons such as the Dharwar, Singhbhum and Bundelkhand exceeding 3 Ga in age, Proterozoic mobile belts and granulite terranes, Gondwana sedimentary sequences rich in organic matter, Mesozoic–Cenozoic ophiolite belts along active and fossil suture zones, the only known active volcanic arc at Barren Island of Andaman, and the fastest-deforming convergent margin in South Asia along the Indo-Burma Range (IBR) (Naqvi 2005; Valdiya, 2016; Mahadevan 2002; Acharyya, 2007). Collectively, these tectonic environments provide geological conditions favourable for multiple H_2-generation mechanisms, including serpentinisation, radiolysis, low-temperature iron oxidation, metamorphic devolatilization, thermogenic reactions, magmatic degassing, and fault-controlled fluid circulation (Sherwood Lollar et al. 2014; McCollom 2016; Zgonnik, 2020; Warr et al. 2021). However, India's natural hydrogen potential remains almost completely uncharacterised through systematic subsurface investigation. The Geological Survey of India (GSI) confirmed natural H_2 in the Andaman and Nicobar Islands in early 2025, confirming the prospectivity of India's ophiolite belts and providing a driver for systematic evaluation of onshore ophiolite systems (Directorate General Hydrocarbon (DGH) 2025).

1.3. Natural hydrogen generation mechanisms in the Indian context

1.3.1 Overview and classification

Ten distinct mechanisms capable of producing molecular hydrogen in the Earth's crust are recognised in the literature. These fall into three broad categories: (i) water-rock redox reactions including serpentinisation, low-temperature iron oxidation, metamorphic dehydration, (ii) energy-driven dissociation of water including radiolysis, mechanochemical generation, thermogenic cracking, and (iii) mantle or biological sources including magmatic degassing, microbial metabolism (Sherwood Lollar et al. 2014; Zgonnik, 2020; McCollom 2016; Truche et al. 2020; Warr et al. 2021). Each of these mechanisms is favoured in a different Indian geological province. Rather than surveying them in isolation here, this study evaluates all ten against the Indian geological inventory within a single weighted framework: the criteria and rating scheme are developed and the resulting mechanism-by-mechanism prospectivity ranking across India is presented in this paper. The remainder of this Introduction establishes why serpentinisation in the ophiolite belts of the Indo-Burma Range emerges from that ranking as one of the country's most promising targets. (Coveney et al. 1987; Telling et al. 2015).

1.3.2 Serpentinisation: the dominant mechanism

Among all recognised mechanisms, serpentinisation of ultramafic rocks is individually capable of producing commercially relevant H_2 fluxes. This mechanism combines large reaction volumes (ophiolite massifs spanning thousands of km²) and high per-kilogram H_2 yields (10–500 mmol/kg depending on Fe content and degree of reaction (McCollom & Bach 2009)). It can sustain production through regeneration for as long as unaltered olivine and circulating water coexist. The essential reaction oxidises ferrous iron in olivine by water, as shown in Eq. 1. (Kelley et al. 2005; Templeton et al. 2024; Wegner and Ernst 1983).

$$2\ Mg_{1.8}Fe_{0.2}SiO_4 + 1.367\ H_2O \rightarrow Mg_3Si_2O_5(OH)_4 + 0.133\ Fe_3O_4 + 0.133\ H_2 \quad (1)$$

This reaction is exothermic ($\Delta H \approx -90$ kJ/mol), generating local heat that may accelerate reaction kinetics in a positive feedback loop. In Fe-rich systems, the Schikorr-type pathway dominates, whereby fayalite reacts with water to produce magnetite, silica, and hydrogen. This reaction (Eq. 2) is analogous to the classical Schikorr reaction for magnetite formation from ferrous hydroxide and therefore represents a key hydrogen-generating pathway distinct from the olivine-serpentinisation reactions discussed above. (Frost 1985).

$$6\ Fe_2SiO_4 + 7\ H_2O \rightarrow 3\ Fe_3O_4 + 6\ SiO_2 + 6\ H_2 \quad (2)$$

Harzburgite and dunite are the dominant lithologies of the Indo-Burma Range (IBR) (also known as the Indo-Myanmar Range) ophiolites. Olivine contents range from 60–95%, with Fe/(Fe+Mg) ratios of 0.08–0.12. These compositions can theoretically generate 30–60 mmol/kg of H_2. Serpentinisation is most efficient between 150 and 350 °C. In the IBR, this temperature range corresponds to depths of ~3–10 km, assuming geothermal gradients of 35–45 °C/km. Direct heat-flow measurements are unavailable in the Manipur Ophiolite Complex. Therefore, in the absence of direct deep-temperature measurements from the Manipur ophiolite, a geothermal gradient of ~25–35 °C/km was adopted as a first-order estimate, guided by corrected bottom-hole-temperature data from the adjacent Upper Assam Basin, where geothermal gradients of ~15–33 °C/km (predominantly ~17–33 °C/km) have been reported (Dutta et al. 2024), together with geothermal gradients characteristic of continental and accretionary-wedge settings. Pollack et al. (1993) reported a global median continental geothermal gradient of ~34 °C/km, which is consistent with the adopted range. Globally, gases emitted from serpentinites record the highest average H_2 concentrations (~21 %) of any continental geological setting. It is surpassed only by mid-ocean-ridge emissions (~24 %) (Zgonnik, 2020).

A mechanically critical feature of serpentinisation is the ~40 % solid-volume expansion, as dense olivine (ρ = 3.3 g/cm³) transforms to serpentine (ρ = 2.5 g/cm³). Under confinement this produces crystallisation pressures up to 300 MPa (Kelemen & Hirth 2012; Plümper et al. 2012), far above the tensile strength of most rocks (~5–10 MPa), driving reaction-induced fracturing that continuously subjects fresh olivine and supports the reaction autocatalytically (Martin and Fyfe 1970).

1.3.3 Chromitite-associated H_2 generation

Recent work at the Bulqizë chromite mine, Albania (Truche et al. 2024), showed that podiform chromitites within ophiolites are associated with significant H_2 occurrences, indicating a potentially dynamic H_2 system. The measured H_2 concentrations reached 84 vol.% in mine workings. The MOC comprises established podiform chromitites in both the Sirohi (Cr# 0.75–0.76) and Gamnom (Cr# 0.65–0.71) varieties, spatially associated with serpentinised peridotites. This represents a geological configuration comparable to Bulqizë, highlighting the MOC as a potential H_2 exploration target, although direct H_2 occurrence remains unconfirmed. (Abrajano et al. 1988; Singh 2008).

1.3.4 Secondary mechanisms: radiolysis, thermogenic, slab dehydration

In ancient cratons where serpentinisation is not present, radiolysis of water by α, β and γ radiation from U, Th and ^{40}K decay creates the principal H_2 source. Holland et al. (2013) documented ancient fracture brines reaching 7.8 mmol/L H_2 in the Canadian Shield. This demonstrates sustained radiolytic hydrogen production over geological timescales. The Singhbhum Craton is the most favourable Indian analogue for this phenomenon because of its Archean age, uranium-bearing lithologies and long-lived crystalline basement (Mukhopadhyay 2001; Saha 1994). In deeply buried sedimentary basins, thermal cracking of highly mature organic matter can also generate H_2 at vitrinite reflectance greater than approximately 2.0% Ro (Seewald 2003; McCollom 2013), although this process remains unverified in the deep Cambay Basin. Beneath the Indo-Burma Range, dehydration of the subducting Indian slab releases large volumes of aqueous fluids into the mantle wedge and overlying crust (Schmidt and Poli 1998; van Keken et al. 2011). These fluids may promote hydration and serpentinisation of ultramafic rocks where suitable lithologies occur, thereby indirectly sustaining H_2 generation, although this mechanism has not yet been demonstrated specifically for the Indo-Burma ophiolites (Deschamps et al. 2013; Merdith et al. 2023; Fryer et al. 1999; Hacker 2008; Mottl et al. 2004; Rüpke et al. 2004; Sherwood Lollar et al. 2007).

1.4 Knowledge gaps and rationale

Despite the rapid global expansion of natural hydrogen research following the characterisation of the Bourakebougou accumulation in Mali (Prinzhofer et al. 2018; Maiga et al. 2023), the Indian subcontinent remains underrepresented in the international prospectivity literature relative to its geological diversity. A recent reconnaissance-level study has screened several Indian geological settings for natural hydrogen potential (Boruah et al. 2025), but national-scale quantitative resource assessment and detailed province-specific modelling remain largely absent. This limited coverage is not attributable to unfavourable geology. India hosts Archean cratons and granitoid–greenstone terranes potentially suitable for radiolytic generation and Fe^{2+}-oxidizing water–rock reactions, extensive Proterozoic mobile belts, organic-rich Gondwana sequences, large igneous provinces, and Mesozoic–Cenozoic ophiolite belts emplaced along both fossil and actively deforming suture zones (Ballentine et al. 2025). The identification of naturally occurring H_2 in the Andaman and Nicobar Islands by the Geological Survey of India in 2025 demonstrates that at least one Indian ophiolitic setting hosts detectable natural hydrogen, although publicly available information does not yet establish accumulation volume, sustainable flow rate or commercial productivity. The occurrence nevertheless provides direct justification for systematic evaluation of Indian ophiolitic terranes. No peer-reviewed, spatially explicit estimate of generated, in-place or technically recoverable H_2 has yet been reported for an onshore Indian ophiolite. The country's natural hydrogen endowment therefore remains quantitatively unconstrained at a time when national policy under the National Green Hydrogen Mission (NGHM) is actively expanding the broader hydrogen-production, infrastructure and utilisation portfolio. The Mission is presently focused on green hydrogen and its derivatives rather than natural hydrogen, but the development of a national hydrogen economy creates a strategic basis for evaluating indigenous geological H_2 as a possible complementary future resource. Three specific gaps follow from this. (Sukumaran 2024).

Three major gaps remain. Firstly, India lacks a comprehensive quantitative and uncertainty-aware framework for evaluating the natural hydrogen generation mechanisms. Previous studies have considered single processes or reconnaissance prospectivity (Boruah et al. 2025). The oxidation of Fe^{2+} in water-rock interactions and water radiolysis is the dominant source of crustal H_2 on a global scale, with thermal, mechanical, magmatic, and biological processes contributing in particular settings (Ballentine et al. 2025). This study evaluates ten specifically defined pathways for H_2 generation/release and identifies the best geological region in India for each pathway.

Second, geomechanical controls have received limited attention in natural hydrogen prospectivity assessment. Serpentinisation and associated H_2 generation in initially low-permeability ultramafic rocks require continued delivery of water to reactive Fe^{2+}-bearing mineral surfaces. Field, microstructural and experimental studies indicate that reaction progress can be strongly influenced by tectonic fracturing, reaction-induced cracking, creation of reactive surface area and maintenance of advective fluid pathways (Andreani et al. 2007; Kelemen & Hirth 2012; Plümper et al. 2012). Reactant delivery and product migration therefore depend on connected fracture networks whose hydraulic conductivity is influenced by effective stress, fault orientation, pore pressure and proximity to frictional failure (Sibson 1994; Barton et al. 1995). Consequently, where protolith fertility, fluid availability and thermal structure are broadly comparable, differences in stress state and connected fracture permeability may discriminate between provinces. This link should be read as a testable hypothesis, not as absolute proof that stress always overrules mineralogy, reaction kinetics, water availability, trapping, or H_2 consumption. In most of the natural hydrogen literature, the assessment of prospectivity is still largely dominated by petrological and geochemical source parameters, although modern models of geological systems emphasise generation, migration, accumulation, and preservation as separate requirements (Etiope, 2023; Ballentine et al. 2025). No peer-reviewed Indian evaluation identified in the current literature search utilized Thermo-Hydro-Mechanical-Chemical coupling (Rutqvist & Stephansson 2003) or rigorously investigated fracture theory or used Coulomb failure analysis in the natural- H_2 context.

Third, no peer-reviewed province-scale volumetric estimate has been reported for an Indian natural hydrogen system. The MOC is highly serpentinised, contains podiform chromitite and is situated in a dynamically deforming region of the India–Myanmar convergent system. This combination of reactive ultramafic protolith, structural permeability and meteoric-water accessibility is in many ways similar to H_2-bearing ophiolitic systems known from regions such as Oman, Albania, Turkey and the Philippines (Etiope, 2023; Truche et al. 2024). Geological parallel implies exploration possibility, not proof of local H_2 or economic viability. The H_2 masses generated, retained and technically recoverable from the MOC have not been previously assessed, leaving policy makers and explorers without a rough estimate of the availability of resources for future data collection or investment decisions.

This study addresses these gaps sequentially. A mechanism-level national framework is developed and used to identify the most favourable Indian province for each of ten operationally defined generation or release pathways. A geomechanical framework is then established to evaluate how stress state, fracture permeability and pore pressure may exert first-order controls on fluid access and H_2 migration across different geological mechanisms. Focusing on the MOC as one of India's most promising targets, published petrological, geochemical, mineralogical, isotopic and structural datasets are integrated with a newly compiled and harmonised literature-derived geochemical database, an original regional Curie-point-depth and heat-flow analysis, a serpentinisation phase-equilibria model, a twelve-criterion prospectivity matrix and a five-stage probabilistic volumetric calculation.

1.5 Objectives and structure

This paper integrates three harmonised lines of analysis. It covers (i) appraisal of all ten crustal H_2 generation mechanisms relevant to India and indicates the provinces where these processes are optimal for generation; (ii) development of a unified geomechanical framework defining the subsurface controls on H_2 generation, migration, and accumulation processes; and (iii) application of this framework, together with an original geochemical database, serpentinisation phase-equilibria model, multi-criteria prospectivity scoring, and five-stage volumetric resource calculation, to the MOC. The MOC is identified herein as one of India's most promising targets within the adopted framework. The specific objectives are:

- Methodically document all ten crustal H_2 generation mechanisms with their thermodynamic, kinetic, and geological requirements, and identify the best Indian H_2 province for each.
- Develop a unified geomechanical (THMC-coupled) framework defining the subsurface controls on H_2 that apply across all mechanism types.
- Analysis of the geological, geochemical, mineralogical, isotopic and structural evidence for natural H_2 prospectivity of the MOC.
- Quantify MOC prospectivity through a 12-criterion scoring matrix, a temperature–pressure serpentinisation model, and a five-stage volumetric H_2 resource estimate.
- Benchmark the MOC against established H_2-producing ophiolites worldwide and define a phased exploration roadmap aligned with National Green Hydrogen Mission (NGHM) of India.

2. Materials and Methods

2.1 Geological Setting of the Study Area

2.1.1 Indo-Burma Orogenic Belt

The Indo-Burma Orogenic Belt (IMOB) (Figure 2) is an NNE–SSW-trending orogenic system shaped by collision of the Indian plate and Eurasian margin, represented locally by the Burma (Myanmar) microplate during the Cenozoic (Mitchell 1993; Acharyya, 2007). The belt constitutes the southern extension of the Indus–Tsangpo Suture Zone. It records a composite history of pre-subduction mid-ocean-ridge spreading, subduction, and arc magmatism within the Neo-Tethyan Ocean (Singh et al. 2024). The western margin of the Indo-Burma Range comprises tectonically dismembered ophiolitic sequences of the Nagaland–Manipur Ophiolite Belt (NMOB) as fault-bounded slices within a regional-scale mélange zone. The IMOB is among the most seismically active regions in India, with annual Mw ≥ 5.0 events (including the 2016 Manipur earthquake, Mw 6.7) potentially influencing fracture permeability and H_2 migration. (Acharyya 2010). (Banerjee et al. 2008).

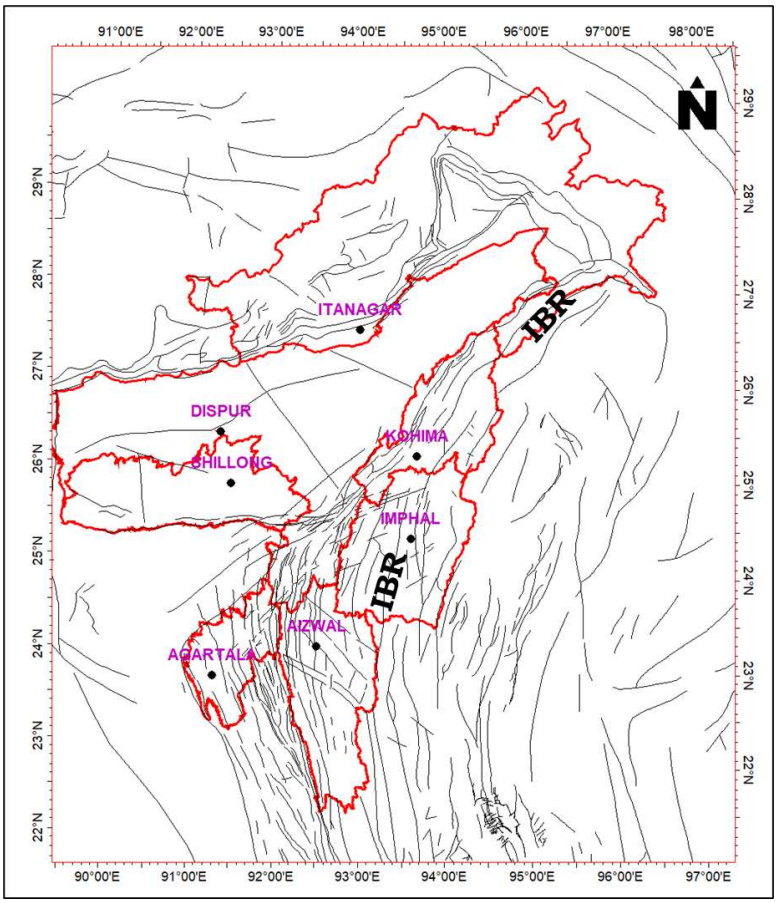


Figure 2. Indo-Burma (Myanmar) Range.

2.1.2 Nagaland–Manipur Ophiolite Belt

The Nagaland–Manipur Ophiolite Belt (NMOB) extends for approximately 500 km in an NNE–SSW orientation across Nagaland and Manipur. It represents remnants of the Neo-Tethyan Ocean floor emplaced during the Indo–Burma collision. Geochemically, the belt is characterised by normal mid-ocean-ridge basalt (N-MORB), enriched mid-ocean-ridge basalt (E-MORB) and supra-subduction-zone (SSZ) magmatic signatures. This is indicative of the geological transition from a spreading ridge to a subduction zone (Sengupta et al. 1989; Khogenkumar et al. 2016; Dey et al. 2018). Lherzolites record low (less than 10%) degree of partial melting of fertile mantle, whereas harzburgites document high melt extraction (up to 17%). (Acharyya 1986). (Ghose et al. 2014). (Singh and Ao 2025).

2.1.3 Manipur Ophiolite Complex: lithostratigraphy

The Manipur MOC is a dismembered ophiolite sequence comprising a tectonic mélange and an olistostromal assemblage, formed at an active plate margin (Evans 1964; Vidyadharan et al. 1989; Acharyya, 2007). The principal lithological units, include serpentinite (dominantly lizardite-, chrysotile-, and antigorite-bearing assemblages replacing dunite and harzburgite), serpentinised harzburgite and lherzolite exhibiting protogranular, mesh, honeycomb, and ribbon textures, dunite pods (olivine Mg# > 0.90), podiform chromitite lenses, cumulate pyroxenites, gabbronorites and gabbros, mafic dykes and pillow basalts, and pelagic marine sediments comprising radiolarian cherts and mudstones (Vidyadharan et al. 1989; Acharyya, 2007; Fareeduddin and Dilek 2015; Singh et al. 2017). Striations and slickenside surfaces throughout the peridotites attest to extensive faulting and shearing associated with both the original oceanic regime and subsequent Himalayan-age deformation.

Table 1: Generalized litho-stratigraphic succession of Manipur, Indo-Burma Range (NE India) Modified after Soibam & Singh (2006) and Kesari (2011). Contact relationships are indicated between successive units; the base of succession is not exposed.

Age	Group	Formation	Lithological description
Recent–Holocene	Quaternary	—	Unconsolidated fluvial and lacustrine deposits: sand, silt, gravel, boulder and clay of the Imphal valley.
~ ~ ~ ~ ~ Unconformity ~ ~ ~ ~ ~			
Mio-Pliocene	Tipam	—	Ferruginous, coarse-grained sandstone with subordinate mottled clay.
Gradational Contact			
Miocene	Surma	Bokabil Bhuban	Alternating shale and siltstone with minor fine-grained sandstone; sandstone increases upward (Bokabil over Bhuban).
~ ~ ~ ~ ~ Unconformity ~ ~ ~ ~ ~			
Oligocene	Barail	Renji Jenam Laisong	Coarse, gritty, massive to well-bedded sandstone showing current bedding and ripple marks, with plant remains, coal streaks and conglomerate lenses.
Gradational Contact			
Eocene	Disang	Upper Disang	Shale, siltstone and greywacke with rhythmite; olistostrome bearing fossils and tectonic slices of ophiolitic rocks.
		Lower Disang	Shale and wacke with rhythmite and minor sandstone bands.
Tectonic Contact			
Cretaceous– Lower Eocene	Oceanic Pelagic Sediments	Lushai	Shale interbedded with red, green and grey chert bearing radiolaria and diatoms, associated wacke and volcaniclastic sediments.
Cretaceous–Early Eocene	Manipur Ophiolite	Ophiolite Suite	Volcanic rocks with flow breccias; gabbro, plagiogranite, pyroxenite, lherzolite, harzburgite, dunite and peridotite variably serpentinised, with disseminated to nodular and massive podiform chromite.
Base not exposed			

2.2 Data sources and geochemical database compilation

This research utilizes existing high-calibre laboratory datasets and amalgamates them into a cohesive analytical structure, eliminating the need for supplementary laboratory examinations. A comprehensive geochemical database was compiled by incorporating previously published whole-rock, mineral-chemical and isotopic analyses of the MOC area in a single organised workbook. The database was prepared from peer-reviewed research papers covering the northern (Ukhrul), central (Nungbi and Gamnom) and southern (Moreh) parts of the MOC and the main ultramafic and mafic lithologies (Ningthoujam et al. 2012; Chaubey et al. 2022; Kingson et al. 2017; Singh et al. 2012). The compiled dataset comprises several published analyses partitioned into two principal populations: (i) whole-rock analyses of serpentinised ultramafic rocks, including serpentinite, harzburgite, dunite, lherzolite and wehrlite, together with mafic lithologies such as pillow basalt, mafic dyke and gabbro; and (ii) published chromium-spinel analyses hosted in harzburgite, dunite and lherzolite. For each whole-rock sample, major-element compositions (SiO_2, TiO_2, Al_2O_3, Fe_2O_3T, MgO, CaO, Na_2O, K_2O, MnO and Cr_2O_3), loss on ignition (LOI), Cr and Ni concentrations, magnesium number [Mg/(Mg+Fe)], olivine forsterite content (Fo), and published estimates of serpentinisation extent were recorded where available. Chromium-spinel datasets include chromium number [Cr/(Cr+Al)], magnesium number [Mg/(Mg+Fe)], Al_2O_3, Cr_2O_3, FeO, MgO, TiO_2 and Fe^{2+}/Fe^{3+} ratios together with associated olivine and pyroxene compositions. The database was designed to record the main lithological diversity of the MOC, not to provide statistically complete spatial sampling of the ophiolite belt.

Tectonic affinity was assigned using published petrological interpretations supported by Cr-spinel Cr#, whole-rock TiO_2, Al_2O_3 and associated discrimination criteria developed for supra-subduction-zone (SSZ), boninitic SSZ, MORB and transitional SSZ–MORB ophiolites (Dick and Bullen 1984; Arai 1994; Kamenetsky et al. 2001; Pearce 2014). No tectonic classification was reinterpreted where the original publications had already reached a conclusion. Within the ultramafic population, published serpentinisation estimates range from 60–97%, MgO from 35.2–44.21 wt.%, Cr from 1200–4572 ppm, Ni from 1800–4138 ppm, TiO_2 from 0.01–0.10 wt.%, and Cr-spinel Cr# from 0.47–0.83. These published compositional ranges define the geochemical envelope used to constrain the serpentinisation phase-equilibria modelling and the subsequent probabilistic volumetric calculations. They are used as geological constraints rather than statistically demonstrative population parameters. All analytical values were retained exactly as reported in the original publications. No recalculation of major-element oxides, mineral formulae, Mg#, Cr#, Fe^{2+}/Fe^{3+} ratios or serpentinisation indices was performed. Likewise, no inter-laboratory normalisation, analytical bias correction or compositional re-standardisation was applied because the constituent studies employed different analytical laboratories, analytical protocols and quality-control procedures. Formal propagation of laboratory analytical uncertainty was therefore not attempted; uncertainty within the prospectivity and volumetric models instead reflects the published compositional ranges and Monte Carlo parameter distributions described in Sections 2.5 and 2.6.

2.3 Method for a unified geomechanical framework for H_2 prospectivity

This section describes the integration of geomechanical and geochemical data for hydrogen prospectivity.

2.3.1 Geomechanics as the master control

The H_2 generation process requires access to fluids to reactive mineral surfaces, or accumulated H_2 to migrate from generation sites to structural traps. Fluid flow in low-permeability crystalline and metamorphic rocks is

generally controlled by fracture networks, and fracture permeability is in turn controlled by the in-situ stress state. Geomechanics may represent a first-order control on fluid access and migration where suitable reactive lithologies already exist in natural H_2 systems. If protolith quality and thermal conditions are comparable, the province with the most mechanically favourable stress state will produce, migrate, and preserve the most H_2. This principle has been demonstrated empirically for serpentinisation by Kelemen & Hirth (2012) and theoretically by Andreani et al. (2007). They showed that reaction rate is fracture-density-limited rather than kinetically limited above 150 °C.

2.3.2 THMC coupling

The geomechanical control on H_2 systems is best formalised through the Thermo-Hydro-Mechanical-Chemical (THMC) coupling framework. It describes the dynamic feedbacks among temperature, fluid flow, stress, and water–rock reactions in the Earth's crust (Rutqvist & Stephansson 2003; Steefel et al. 2015). Each component exerts feedback on the others:

- **Thermal (T):** Subsurface temperature controls the kinetics of serpentinisation, radiolysis, and thermogenic reactions. Serpentinisation is an exothermic hydration reaction. This reaction is capable of generating sufficient heat to locally sustain reaction progress under favourable conditions (Sleep et al. 2004; Emmanuel & Berkowitz 2006; Evans 2008). Regional heat-flow values reported from the Indo–Burma Range are of around 75–95 mW m^{-2}. This indicates that ultramafic rocks may exist in the favourable serpentinisation temperature window at depths of approximately more than 3 km (Rao et al. 2003).
- **Hydraulic (H):** In tectonically active suture zones, pore pressures transient to long lasting, close to lithostatic, reduce the effective normal stress on faults and fractures and the frictional resistance, allowing fracture opening or fault reactivation. Continued fluid production and/or influx may gradually restore pore pressure until failure occurs, producing sudden crack widening and episodic fluid release. Subsequent sealing by mineral deposition or compaction enables pressure to accumulate again. This persistent fault-valve mechanism can preserve or intermittently reactivate fracture permeability over geological epochs, enabling long-lasting and repeated fluid–rock interactions (Sibson 1992; Ingebritsen et al. 2006; Hubbert and Rubey 1959; Neuzil 2003; Terzaghi 1943).
- **Mechanical (M):** The critical stress state of the fractures and thus the hydraulic conductivity is controlled by the in-situ stress field (Zoback 2007). Serpentinisation is the hydration of olivine and pyroxene, accompanied by a solid volume expansion of ~20–40%, which results in the generation of crystallisation stresses that lead to reaction-driven fracturing, increased permeability and enhanced ongoing flow of reactive fluids (Jamtveit et al. 2008; Plümper et al. 2012; Kelemen & Hirth 2012).
- **Chemical (C):** Water-rock interactions gradually change mineral compositions, density, porosity, elastic properties and rock integrity, thus affecting the hydraulic and mechanical dynamics of the system (O'Hanley 1996; Frost & Beard 2007). Serpentinisation leads to the precipitation of magnetite, which significantly increases magnetic susceptibility and remanent magnetization, providing a key geophysical signature for locating serpentinisation extent and hydrogen-producing reaction zones (Toft et al. 1990; Evans 2004).

2.3.3 Critically stressed fractures and the Coulomb criterion

The critically stressed fracture concept (Barton et al. 1995) provides the mechanical relation between in-situ stress and fracture permeability. A fracture is considered critically stressed when its shear stress τ is close to the frictional strength limit defined by Byerlee's law ($\mu s \approx 0.6–0.85$). The Coulomb Failure Function (CFF), which quantifies the proximity of a fault or fracture to failure, is defined in Eq. (3):

$$CFF = \tau - \mu s \cdot \sigma'n = \tau - \mu s(\sigma n - Pp) \quad (3)$$

Table 2. Geomechanical parameters controlling natural H_2 generation, migration, and accumulation across all mechanism types, together with representative screening criteria applicable to the Indo-Burma Range and MOC.

Parameter	**Role in H_2 generation**	**Representative screening criterion**	**Measurement proxy**	**Key references**
Effective normal stress (σ′n)	Controls fracture aperture and fluid access	Low effective normal stress	Hydraulic fracturing; leak-off tests; sonic logs	Sibson (1994); Barton et al. (1995); Alam et al. 2019
Differential stress (σ_1–σ_3)	Promotes fracture reactivation and permeability anisotropy	Elevated differential stress	Focal mechanisms; borehole breakouts	Zoback (2007); Townend, Zoback (2000)
Fracture density (P_{32})	Provides fluid pathways for serpentinisation and H_2 migration	High connected fracture density	FMI; lineament density; core logging	Andreani et al. (2007); Kelemen & Hirth (2012)
Stress ratio (k = σH/σV)	Influences fault stability and migration pathways	Transpressional/compressional stress regime	Breakouts; GPS; moment tensors	Zoback (2007); Heidbach et al. (2025)
Crystallisation pressure (ΔPcryst)	Reaction-induced expansion generates fractures	ΔPcryst exceeding host-rock tensile strength	Microstructure; laboratory experiments	Jamtveit et al. (2008); Plümper et al. (2012)
Temperature (T)	Controls serpentinisation kinetics and H_2 generation	150–350°C	Thermochronology; Curie depth; heat flow	McCollom & Bach (2009); Klein et al. (2013)
Fault reactivation (CFF)	Critically stressed faults enhance fluid flow	Near-critical fault stress	Stress inversion; seismicity	King et al. (1994); Zoback (2007)

When CFF is greater than or equal to zero, frictional sliding in an idealized context may occur; however, dilatation and increased permeability are not assured. In optimal parallel-plate flow, fracture transmissivity correlates roughly with the cube of hydraulic aperture; a separate stress–aperture closure relationship is necessary. In the transpressional Indo-Burma Range, the peak horizontal compressive stress (σH) is indicated by the sensitivity baseline of N55°E, instead of the locally evaluated stress azimuth, the regional tectonic context of the GPS research (Gahalaut et al. 2013; Kundu & Gahalaut, 2013). The comparison of regional structures shows that ophiolite faults are heterogeneous and that particular shallow MOC fault planes cannot

be assumed to be critically stressed without local depth-dependent stress levels, pore pressures and observed fault orientations. The geomechanical parameters controlling the natural hydrogen generation cycle and associated parameters are provided in Table 2. The lineament density, a proxy for fracture density is presented in Figure 3.

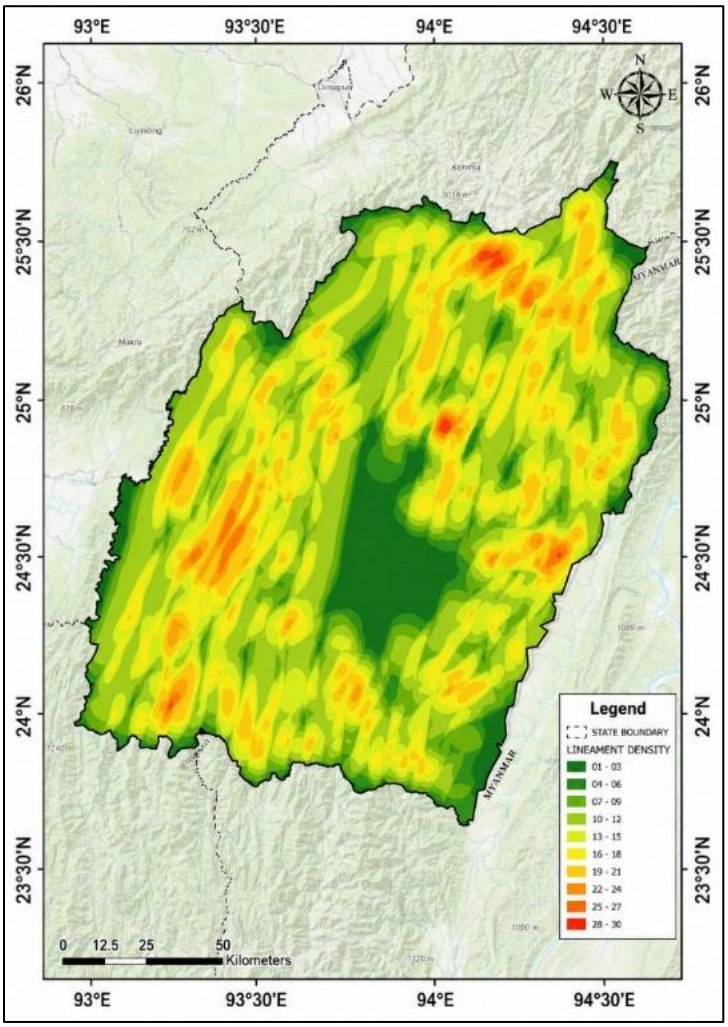


Figure 3. Lineament density distribution highlighting possible major fracture corridors in the Manipur region.

2.4 Serpentinisation phase equilibria and H_2 yield model

2.4.1 Temperature–pressure stability of serpentine minerals

The serpentine polymorphs like lizardite, chrysotile and antigorite have distinct pressure–temperature stability fields that govern both the style and productivity of serpentinisation. Lizardite and chrysotile dominate at low temperature (<300 °C) and are the principal MOC assemblage, whereas antigorite stabilises at higher temperatures (200–700 °C) and pressures. Figure 4 plots these fields together with the modelled MOC geotherm (35 °C/km, representing the upper limit of the adopted 25–35 °C/km range and the locus of peak H_2 generation. The MOC geotherm passes through the lizardite and lower-antigorite fields within the optimal H_2 window (shaded), consistent with the observed lizardite–chrysotile–antigorite assemblage.

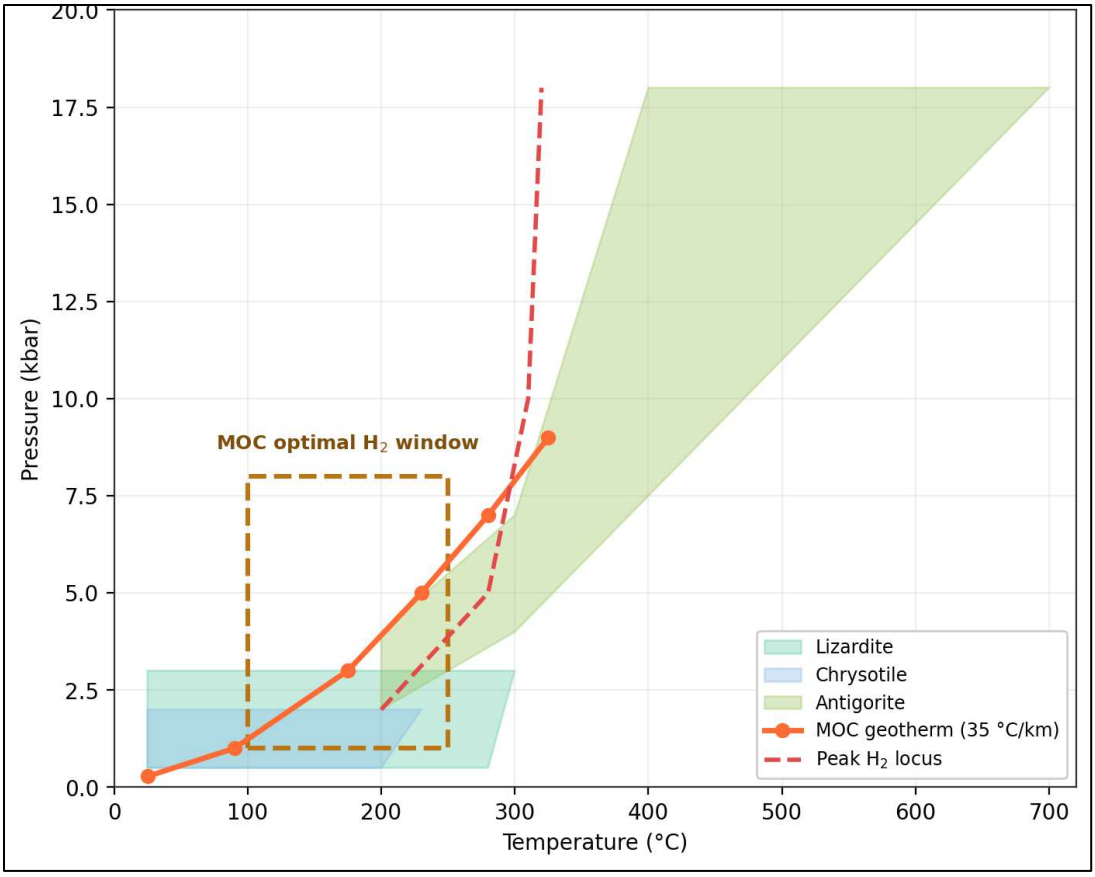


Figure 4. Pressure–temperature phase diagram showing serpentine-mineral stability fields, the MOC geothermal path (35 °C/km, orange), the peak-H_2 generation locus (dashed red), and the MOC Optimal H_2 window (dashed amber box, 100–250 °C, 1–8 kbar). The geotherm traverses the lizardite and lower-antigorite fields, matching the observed MOC mineral assemblage. (Ulmer and Trommsdorff 1995).

2.4.2 Temperature-dependent H_2 yield

H_2 yield from serpentinisation is strongly temperature-dependent, rising from negligible values below 100 °C to a maximum near 300 °C before collapsing above 400 °C as serpentine destabilises to talc + olivine. Applying an empirical kinetic model (after McCollom & Bach 2009; Etiope, 2024) across a range of pressures yields the curves. At the MOC modelled lithostatic pressure range at 3–8 km (~0.8–2.1 kbar), the optimal 100–300 °C window is accessible at 3–8 km depth given the IBR geotherm, which captures the bulk of the achievable H_2 yield.

2.5 Multi-criteria prospectivity scoring framework

2.5.1 Mechanism-level prospectivity rating scheme

Before site-specific scoring (Sections 2.5.2-2.5.3), each of the ten generation mechanisms was assigned a national prospectivity rating on a five-point ordinal scale (★ to ★★★★★). The rating for each mechanism reflects the joint favourability of four factors in its optimal Indian province: the availability and volume of suitable source rock or precursor; the thermal and geochemical conditions required for the reaction to proceed at a meaningful rate; the structural or hydrogeological pathways available for fluid circulation and product

migration; and the strength of supporting evidence, whether direct observation, global analogue, or inference. A mechanism was rated ★★★★★ only where all four factors are strongly satisfied in a well-defined Indian location, and ★ where the mechanism is geologically permissible but volumetrically minor, poorly located, or rapidly self-consuming. The "best Indian location" recorded for each mechanism in Table 12 (Section 3.8) is the province in which that mechanism's four factors are jointly maximized, not merely a place where the host lithology occurs.

The scheme is a structured expert weighting applied to published evidence rather than a purely subjective ordering: the serpentinisation ratings draw on the ophiolite and forearc literature, the radiolysis and thermogenic ratings on documented Indian craton and basin settings, and the analogue-dependent ratings on established global occurrences. The ordinal ratings are comparative and are not interconvertible with the continuous prospectivity index P of Equation (9); they serve to prioritize mechanisms nationally, whereas Equation (9) scores locations.

2.5.2 Scoring framework

To quantify and compare H_2 prospectivity, a weighted multi-criteria scoring matrix combining twelve geological, structural, and exploration criteria, grouped into source, migration, accumulation, validation, and risk categories, was applied. Each criterion is scored 0–10 and weighted by its evaluated importance, yielding a composite prospectivity score. This framework operationalizes the Serpentinisation Potential Index (SPI) and Hydrogen Prospectivity Index (HPI)

The Serpentinisation Potential Index is defined in Eq. (4):

$$SPI = f_{ol}\, k_f\, T_C\, q_f \tag{4}$$

The composite Hydrogen Prospectivity Index (HPI) is defined in Eq. (5):

$$HPI = (\Sigma^{5}_{i=1}\, w_i\, SI_i)\, \eta_m\, \eta_t \tag{5}$$

Where, f_{ol} is the olivine modal fraction, k_f is the fracture permeability, T_C is a dimensionless thermal-compliance factor, q_f is the fluid flux, SI_i denotes the normalised sub-index scores (Serpentinisation Intensity, Fluid Access, Thermal Compliance, Preservation Potential and Analogue Match), w_i denotes the corresponding weights (0.30, 0.25, 0.20, 0.15 and 0.10; $\Sigma w_i = 1$), and η_m and η_t are the migration and trap efficiencies ($0 \le \eta \le 1$), respectively. All input variables are normalised to the interval [0, 1] prior to combination, ensuring that both indices are dimensionless and bounded. For regional prospectivity ranking, migration efficiency (η_m) and trap efficiency (η_t) were assumed equal to unity because of the absence of site-specific subsurface calibration data. Consequently, the operational HPI used in this study reduces to the weighted-sum formulation of Eq. (6). The indices are heuristic screening tools rather than physically derived predictive models. The five sub-indices are composite categories derived from the twelve detailed criteria.

2.5.3 Scoring criteria and weighting

Twelve criteria were considered to capture the full natural hydrogen system including source, generation, migration, accumulation, and exploration readiness. Each zone is scored 0–10 on every criterion, and the composite HPI is calculated as the weighted sum as provided in Eq. 6:

$$HPI = \Sigma\, (S_i \times W_i),\ \ i = 1 \ldots 12 \tag{6}$$

Where, S_i is the score for criterion i and W_i its weight (weights sum to unity). The weights, summarized in Table 3, place utmost importance on source-rock quality and serpentinisation potential. These two factors most strongly govern H_2 generation capacity. This is followed by active tectonics, which controls fluid access and migration.

Table 3. Twelve-criterion weighted scoring framework for natural hydrogen prospectivity assessment. The criteria encompass hydrogen source potential, generation conditions, migration pathways, accumulation and preservation potential, geological analogue correspondence, and exploration maturity. Each criterion is scored on a scale of 0–10 and multiplied by its assigned weight to derive the composite prospectivity score.

#	Criterion	Category	Weight	Scoring basis (0–10)
C1	Ultramafic rock volume	Source	13%	Regionally extensive/thick ultramafic–ophiolitic body = 9–10; moderate extent = 6–8; limited occurrence = 3–5; negligible/absent = 0–2
C2	Serpentinisation degree	Source	14%	Pervasively serpentinised ultramafic rocks = 9–10; moderate/partial serpentinisation = 6–8; weak serpentinisation = 3–5; negligible = 0–2
C3	Fe^{2+} content in protolith	Source	9%	High abundance of reactive Fe^{2+}-bearing minerals = 9–10; moderate = 6–8; low = 3–5; very low/absent = 0–2
C4	Olivine modal content	Source	7%	Olivine-rich ultramafic rock (>60%) = 9–10; 40–60% = 7–8; 20–40% = 4–6; <20% = 1–3
C5	Fault/fracture network	Migration	11%	Dense, interconnected and deep-reaching fault/fracture system = 9–10; moderate connectivity = 6–8; sparse/poorly connected = 3–5; negligible = 0–2
C6	Seismicity	Migration	7%	Highly active tectonic/seismic domain = 9–10; moderately active = 6–8; low activity = 3–5; tectonically stable = 0–2
C7	Geothermal gradient	Migration / Generation	6%	Thermal regime compatible with serpentinisation, approximately 150–350 °C at relevant depth = 9–10; partly favourable = 6–8; marginal = 3–5; unfavourable = 0–2
C8	Trap geometry	Accumulation	9%	Well-defined structural/stratigraphic closure with demonstrable storage volume = 9–10; probable trap = 6–8; poorly constrained = 3–5; no recognised trapping geometry = 0–2
C9	Cap-rock potential	Accumulation	8%	Regionally continuous, low-permeability competent seal = 9–10; locally effective seal = 6–8; uncertain/discontinuous seal = 3–5; ineffective/absent seal = 0–2
C10	Hydrogeology	Accumulation / Fluid access	5%	Strong meteoric/hydrothermal recharge with favourable subsurface circulation = 9–10; moderate fluid access = 6–8; restricted circulation = 3–5; very limited fluid access = 0–2
C11	Analogue match	Validation	5%	Strong correspondence with documented natural hydrogen systems such as Oman/Bulqizë = 9–10; partial analogue = 6–8; weak analogue = 3–5; no meaningful analogue = 0–2
C12	Exploration maturity	Risk / Validation	6%	Direct H_2 measurements, repeated surveys and subsurface confirmation = 9–10; preliminary geochemical/geophysical evidence = 6–8; reconnaissance only = 3–5; essentially unexplored = 0–2
	Total		100%	

Weights were assigned through expert judgement and geological reasoning. As a sensitivity analysis, individual weights were varied by ±20% with the total normalized weight maintained. This establishes sensitivity of the overall MOC composite score, not robust sub-area rank order, because a complete zone-by-criterion scoring matrix is unavailable.

2.6 Five-stage volumetric methodology

Gross rock volume was converted to rock mass using a representative ultramafic-rock bulk density of 2.7 t m^{-3}. Generated hydrogen mass was then estimated from the effective serpentinised volume, density, and adopted hydrogen yield factor. The calculation is intended as an order-of-magnitude screening assessment rather than a formal resource estimate. A conservative recovery factor of 1.5–5% was adopted for screening-level evaluation because hydrogen recoverability in natural systems remains poorly constrained and no production analogue exists for the MOC. The adopted yield of 0.95 mol H_2 t^{-1} represents a conservative basin-scale effective yield used for volumetric screening and should not be confused with the peak reaction yields, which represent idealized temperature-dependent reaction potential under favourable serpentinisation conditions. The estimated in-place and recoverable H_2 resource of the MOC is derived through a five-stage volumetric cascade. It comprises the following five steps:

(1) gross rock volume from ophiolite areal extent and thickness;

(2) net ultramafic rock volume;

(3) effective serpentinised volume;

(4) H_2 generation potential from the stoichiometric/kinetic yield; and

(5) recoverable H_2 under conservative and optimistic recovery factors.

2.7 Scenario-based three-dimensional fault stability and fracture transmissivity

The MOC lacks site-specific measurements of the three principal stresses, pore pressure, hydraulic fracture aperture and permeability. The calculations presented here are therefore sensitivity tests, not estimations resulting from local observations. The original N50–60°E shortening direction is represented by an $S_{H\max}$ azimuth of N55°E. At 2.5 km depth, the reference case assumes $S_{H\max} = 80$ MPa, $S_v = 65$ MPa, $S_{h\min} = 45$ MPa, $P_p = 25$ MPa, zero cohesion and a friction coefficient of 0.60. None of these magnitudes has been measured in the MOC. In the WSM 2025 data for 24–26°N and 93–95°E, six C-quality focal mechanisms give $S_{H\max}$ azimuths of 13°, 23°, 24°, 26°, 28° and 37° (axial mean N25.17°E) at depths of 34.8–49.6 km. A separate C-quality borehole-breakout record west of the main targets gives N131°E at 2.05 km. Given their different depths and locations, these observations are not averaged together. The N55°E case is taken for comparison, and N25.17°E is tested using the same assumed stress magnitudes. The WSM observations constrain stress orientation, not shallow stress magnitudes in the target area (Heidbach et al., 2025; Heidbach et al. 2016).

In east–north–down coordinates, with compression taken as positive, the stress tensor is written as equation (7).

$$\boldsymbol{\sigma} = S_{H\max}\mathbf{e}_H\mathbf{e}_H^{\mathrm{T}} + S_{h\min}\mathbf{e}_h\mathbf{e}_h^{\mathrm{T}} + S_v\mathbf{e}_z\mathbf{e}_z^{\mathrm{T}}, \quad \mathbf{e}_H = (\sin A, \cos A, 0), \quad \mathbf{e}_h = (\cos A, -\sin A, 0). \quad (7)$$

Here A is the clockwise azimuth from north. For a fracture normal $\mathbf{n}$, the traction is $\mathbf{t} = \boldsymbol{\sigma}\mathbf{n}$, normal stress is $\sigma_n = \mathbf{n}^{\top}\boldsymbol{\sigma}\mathbf{n}$, and shear stress is $\tau = \| \mathbf{t} - \sigma_n \mathbf{n} \|$. The additional pore pressure needed to reach the assumed Coulomb slip criterion is written in equation (8).

$$\Delta P_{\mathrm{crit}} = \sigma_n - \frac{\tau - c}{\mu} - P_p. \quad (8)$$

Strike and dip are sampled at 5° intervals over 0–175° and 10–90°, respectively. A negative ΔP_{crit} means that the idealized plane is unstable under the specified inputs; it is not evidence of slip on a mapped MOC fault.

Fracture opening is assessed with an assumed exponential closure law, $b_h(\sigma_n') = b_{\mathrm{res}} + (b_0 - b_{\mathrm{res}})\exp(-\sigma_n'/K)$, where $\sigma_n' = \sigma_n - P_p$, $b_{\mathrm{res}} = 10\,\mu\mathrm{m}$, $b_0 = 100\,\mu\mathrm{m}$ and $K = 20$ MPa. For an imposed pressure increase ΔP, the relative transmissivity from the parallel-plate cubic law is given in equation (9).

$$\frac{T(\Delta P)}{T(0)} = \left[\frac{b_h(\sigma_{n,0}' - \Delta P)}{b_h(\sigma_{n,0}')}\right]^3. \quad (9)$$

Initial effective normal stresses of 20, 35 and 50 MPa are considered for pressure increments of 0–15 MPa. The aperture parameters are not adjusted, and the cubic-law result only shows the mechanical sensitivity of an ideal fracture. It does not determine field-scale connectivity, hydrogen concentration or production potential. The broader relation between joint deformation and conductivity is discussed by Barton et al. (1985).

2.8 Ranking uncertainty and identifiability

Here we use the twelve MOC criterion scores [9, 9, 9, 8, 9, 9, 8, 8, 7, 8, 9, 6] and weights [0.13, 0.14, 0.09, 0.07, 0.11, 0.07, 0.06, 0.09, 0.08, 0.05, 0.05, 0.06]. For 100000 Monte Carlo samples, each weight is multiplied independently with U(0.8,1.2) with fixed random seed and the resulting weights are normalized to sum to one. This HPI distribution is a result of only measuring the sensitivity to weight, with the twelve subjective criterion scores held constant. This is not a valid probability distribution for the abundance of hydrogen. The five reported aggregate HPI values (8.06, 7.98, 7.93, 7.44, 6.46) are applied in a separate explicitly provisional sub-area ranking uncertainty test. We add to each reported aggregate score independently distributed zero-mean Gaussian perturbations of standard deviation 0.2, 0.4 or 0.8 score units. Simulated scores are clipped to [0,10] and ranks recomputed. These arbitrary, clearly labeled scenarios quantify how easily the close top-three ranks can be reversed, but are not calibrated as uncertainty probabilities based on empirical data and do not reproduce an independent geochemical assessment.

3. Results

3.1. Geochemical, Mineralogical and Isotopic Evidence

3.1.1 Pervasive serpentinisation

Serpentinisation is pervasive and volumetrically dominant in the MOC, where serpentinite is the most voluminous litho-unit of a dismembered, thrust-imbricated sequence (Evans 1964; Vidyadharan et al. 1989; Ningthoujam et al. 2012; Ghosh et al. 2014). Petrography and Raman spectroscopy confirm serpentinised ultramafic-cumulate and peridotite protoliths (Ningthoujam et al. 2012), with a lizardite–chrysotile-dominant, antigorite-subordinate assemblage recording moderate- to low-temperature hydration (Singh et al. 2013). Protogranular textures grading to mesh, hourglass and ribbon textures document progressive replacement of

olivine and orthopyroxene, the Fe-bearing phases driving H_2 generation; Ni-serpentine (népouite) with associated magnetite marks the same Fe^{2+}-oxidation pathway (Ovung et al. 2017). A depleted, subduction-influenced peridotite protolith is confirmed by whole-rock, Cr-spinel and Nd-isotope data (Singh 2013; Pal et al. 2014; Kingson et al. 2017; Chaubey et al. 2022; Lamzamuan et al. 2024), while active India–Myanmar convergence sustains the fracturing and fluid flux that maintain the reaction (Acharyya, 2007). Estimated serpentinisation of 70–97 % places the MOC at the high end of the global ophiolite spectrum.

3.1.2 Whole-rock geochemistry

Major-element geochemistry of Manipur Ophiolite Complex ultramafic rocks is distinctive of highly depleted upper-mantle residues with high H_2-generation potential. The extremely high Ni (~1960 ppm) and Cr (~2005 ppm) with low TiO_2 (~0.12 wt %) are diagnostic of residual mantle peridotites that experienced high degrees of melt extraction. This left olivine-rich, Fe^{2+}-bearing residues as the ideal substrate for serpentinisation-driven H_2. Figure 5 compares the major-oxide chemistry of the principal MOC lithologies, showing the sharp compositional separation between the ultramafic source rocks (high MgO, low Al_2O_3/CaO) and the subordinate mafic units. The major-element and trace-element compositions of representative ultramafic and mafic rocks from the Manipur Ophiolite Complex are summarized in Table 4.

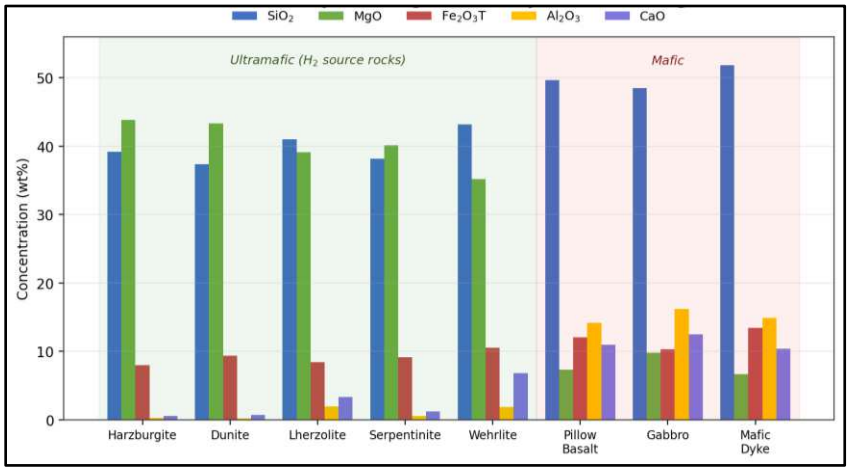


Figure 5. Whole-rock major-oxide geochemistry of the principal MOC lithologies. Ultramafic units (left, green field) combine high MgO with low Al_2O_3 and CaO, the diagnostic signature of depleted, olivine-rich H_2 source rocks; mafic units (right, red field) are compositionally distinct. Compiled from Ningthoujam et al. (2012), Devi and Singh (2011), and Singh et al. (2013).

Table 4. Whole-rock major-element and compatible trace-element geochemistry of MOC ultramafic rocks (after Devi and Singh 2011; Singh NI et al. 2013; Ningthoujam et al. 2012).

Rock unit	MgO (wt%)	Cr (ppm)	Ni (ppm)	TiO_2 (wt%)	CaO (wt%)	Serp. %
Ultramafic tectonite (N. MOC)	~32	~2005	~1960	~0.12	~6.56	—
Serpentinised harzburgite	38–45	1800–2400	1600–2200	0.08–0.15	0.01–0.47	82–85
Serpentinised lherzolite	36–42	1500–2000	1800–2100	0.10–0.20	n.d.	70–72
Dunite pods	40–46	1900–2500	2100–2600	<0.10	0.01–0.47	88–90
Serpentinite (mesh)	39–41	2650–2800	3050–3200	0.02–0.03	1.1–1.3	95–97

3.1.3 Chromian spinel chemistry and tectonic discrimination

Chemistry of chromian-spinel provides two-fold evidence for H_2 prospectivity. It also limits the amount of partial melting that controls the amount of olivine. The presence of high-Cr chromitite pods confirms the lithological configuration as serpentinized peridotite + podiform chromitite and is considered the most productive configuration for geological H_2. Electron-microprobe analyses show two main chromitite varieties. The Sirohi-type (Cr# 0.75–0.76, Al_2O_3 12.2–12.4 wt %) shows boninitic parentage, and the Gamnom-type (Cr# 0.65–0.71, Al_2O_3 15.7–19.0 wt %) shows transitional affinity between IAT and boninite (Pal et al. 2014). In general, MOC chromian spinels (Cr# 0.60–0.82, Mg# 0.54–0.74) fall precisely within the compositional field of the Bulqizë ophiolite, Albania, where H_2 concentrations >50 vol % were directly measured (Truche et al. 2024). Discrimination diagram is shown in Figure 6. The mineral-chemical characteristics of chromian spinels and their implications for the tectonic affinity of the Manipur Ophiolite Complex are presented in Table 5.

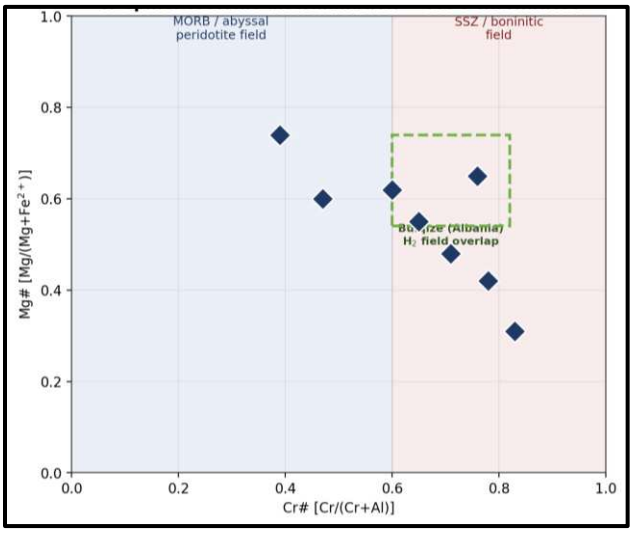


Figure 6. Cr# versus Mg# discrimination diagram for MOC Cr-spinels. Samples span the MORB and SSZ/boninitic fields; the high-Cr# chromitites (Sirohi and Gamnom types) plot within the dashed green field that coincides with the Bulqizë (Albania) chromitite compositions, where >50 vol % H_2 has been measured in mine workings. Data after Pal et al. (2014) and Ghosh et al. (2014).

Table 5. Chromite and chromitite geochemistry of the Manipur Ophiolite Belt with tectonic and H_2 prospectivity implications (after Pal et al. 2014; Devi and Singh 2011; Ghosh et al. 2014).

Chromitite type	Cr#	Mg#	Al_2O_3 (wt%)	Tectonic implication
Sirohi-type (massive)	0.75–0.76	0.54–0.74	12.2–12.4	Boninitic / SSZ
Gamnom-type (massive)	0.65–0.71	0.55–0.70	15.7–19.0	IAT–SSZ transition
Chromite in dunite pods	~0.60	n.d.	20.7–21.2	Moderate partial melt
Accessory Cr-spinel (peridotite)	0.38–0.39	High	34–35	Fertile MORB mantle
Cr-spinel in massive chromitite	0.60–0.82	0.54–0.74	9.9–20.6	Boninitic melt

3.1.4 Hydrothermal alteration: Népouite

A particularly compelling line of evidence is the discovery of népouite. It is a Ni-rich serpentine mineral (NiO = 33.4–33.9 wt %; SiO_2 = 37.55–38.96 wt %; MgO = 14.83–16.89 wt %) in the Ukhrul–Nungbi sector (Kingson et

al. 2017). Ultramafic rocks are required to facilitate efficient hydrothermal fluid flow associated with H_2 generation. The same hydrothermal processes that drive serpentinisation also promote the production of H_2. The presence of népouite suggests a long-term fluid–rock interaction, sufficient to completely serpentinise the protolith and to transport and redeposit Ni in hydrothermal fluids. This is a simple petrographic proxy for H_2-productive serpentinisation conditions described worldwide (Barnes et al. 1978; Neal and Stanger 1983; Neal and Stanger 1985).

3.1.5 Nd-isotope systematics

Nd-isotope measurements on serpentinised peridotites (Kingson et al. 2017) show εNd(t) values between −7.6 and +10.4 in harzburgite and lherzolite. The La/Yb versus εNd(t) correlation is well-matched with progressive addition of subduction-derived fluids to a depleted mantle reservoir. It advocates that external fluids invaded the mantle wedge of the MOC at depth, and produced the conditions of fluid–rock interaction necessary for H_2 production. The published Nd-isotope compositions of the Manipur Ophiolite Complex and their implications for mantle-source characteristics are summarized in Table 6.

Table 6. Nd-isotope systematics of the MOC and implications for source mantle and subduction-fluid interaction (after Kingson et al. 2017; Singh et al. 2024).

Sample type	εNd(t) range	Interpretation	Reference
Serpentinised harzburgite	−7.6 to +10.4	Subduction-fluid metasomatized depleted mantle	Srivastava et al. (2017)
Serpentinised lherzolite	+2.4 to +8.1	Depleted mantle / MORB affinity	Srivastava et al. (2017)
Mafic dykes (N-MORB)	+6.0 to +9.5	Depleted MORB mantle source	Kingson et al. (2017)
Gabbro (E-MORB)	+3.0 to +7.0	Enriched mantle plume mixing	Kingson et al. (2017)

3.2 Depth–temperature controls on serpentinisation and H_2 yield

3.2.1 Modelled serpentinisation conditions and H_2 yield

Modelled temperature-dependent H_2 yield (mmol/kg rock) at three pressures is provided in Figure 7. The yield peaks near 300 °C and falls sharply above 400 °C as serpentine breaks down. The shaded amber band marks the MOC optimal window (100–300 °C); the 5 kbar curve is an elevated-pressure sensitivity case rather than the MOC mean reaction pressure.

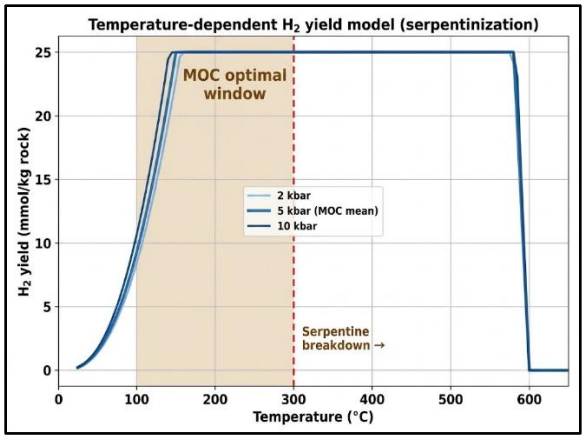


Figure 7. Modelled temperature-dependent H_2 yield (mmol/kg rock) at three pressures.

3.2.2 Depth–temperature structure of the MOC reaction zone

The coincidence between calculated H_2 production and the local geothermal structure determines the depth interval at which active serpentinisation is expected. Figure 8 shows the depth-temperature curve for three geothermal gradients around the IBR. The average gradient of 35 °C/km in the MOC means that the ideal H_2 zone of 100-300 °C is at a depth of about 2-8 km. The base of the ophiolite (3-5 km) is well within this productive range and accessible by conventional exploration drilling. (Pasquale et al. 2017).

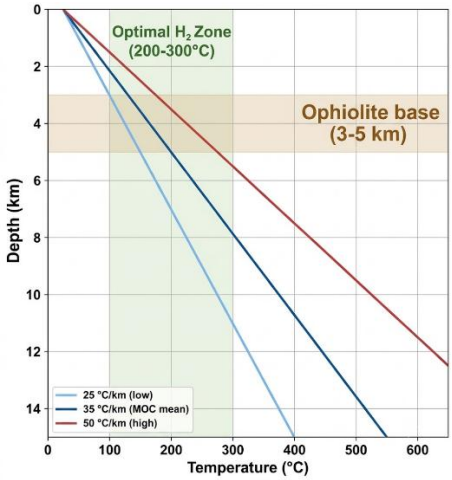


Figure 8. Depth-temperature profile of MOC at three geothermal gradients (25, 35, 50 °C/km). The ideal H_2 zone (green band; 100–300 °C) intersects the ophiolite base (amber band; 3–5 km) at the MOC mean gradient, putting the most productive serpentinisation interval within the reach of conventional drilling.

3.3 MOC intra-belt prospectivity ranking

3.3.1 MOC prospectivity scores and intra-belt ranking

Twelve-criterion natural hydrogen prospectivity radar (Figure 9) for the MOC shows high scores for source-rock attributes, including ultramafic rock volume, degree of serpentinisation, Fe^{2+} content and olivine modal fraction, as well as for migration-related factors such as fault/fracture density and seismicity, together with analogue match. The principal limitations are low exploration maturity and comparatively weaker trap and cap-rock characterisation.

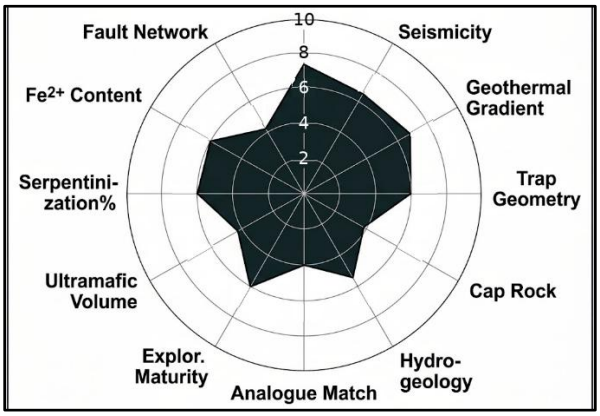


Figure 9. Twelve-criterion natural hydrogen prospectivity radar for the MOC.

Table 7. Weighted multi-criteria prospectivity scoring matrix for the MOC (max composite = 10).

Criterion	Category	Weight	Score	Rating
Ultramafic rock volume	Source	13 %	9	Excellent
Serpentinisation degree	Source	14 %	9	Excellent
Fe^{2+} content in protolith	Source	9 %	9	Good
Olivine modal content	Source	7 %	8	Good
Fault / fracture density	Migration	11 %	9	Excellent
Seismicity level	Migration	7 %	9	Excellent
Geothermal gradient	Migration	6 %	8	Good
Trap geometry	Accumulation	9 %	8	Moderate
Cap-rock potential	Accumulation	8 %	7	Moderate
Hydrogeology	Accumulation	5 %	8	Moderate
Analogue comparison	Validation	5 %	9	Excellent
Exploration maturity	Risk	6 %	6	Very low
Weighted composite	**—**	**100 %**	8.39	**Excellent tier**

3.3.2 Intra-belt sub-area ranking

Disaggregating the MOC into its integral sectors and scoring each on source, migration and trap components produces the ranking presented in Figure 10 and Figure 11. The Ukhrul–Nungbi sector and the central mélange zone emerge as Priority 1 targets. This is because of the highest source and migration scores. The Gamnom–Shangshak sector ranks closely behind, while the Moreh (southern MOC) and Churachandpur sectors form Priority 2 and Priority 3 targets respectively.

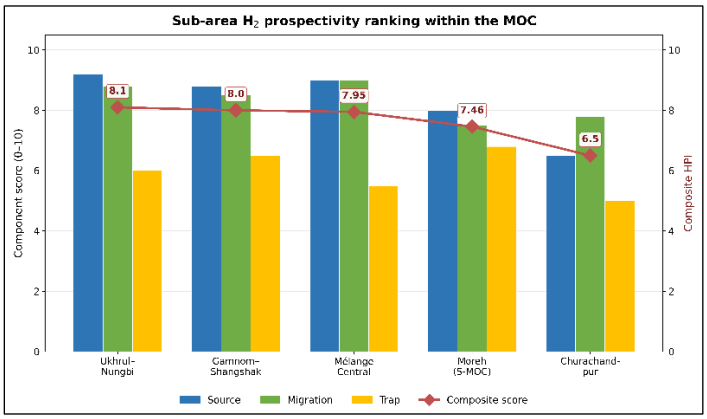


Figure 10. Sub-area prospectivity ranking within the MOC. Bars show source, migration and trap component scores; the red line tracks the composite HPI. Ukhrul–Nungbi, Gamnom–Shangshak and the central mélange zone are the highest-ranked sectors within the adopted framework.

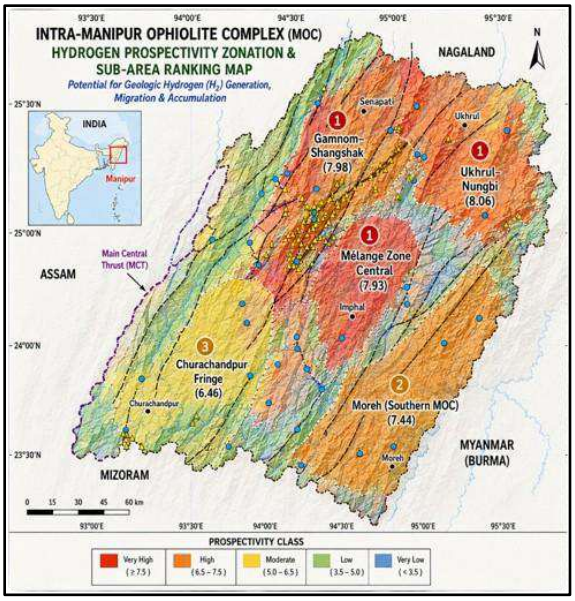


Figure 11. Sub-area prospectivity ranking within the MOC

Table 8. Intra-MOC sub-area prospectivity ranking with composite scores and priority classification.

Sub-area / sector	Lat (°N)	Lon (°E)	Composite	Priority
Ukhrul–Nungbi	25.10	94.35	8.06	Priority 1
Gamnom–Shangshak	25.25	94.50	7.98	Priority 1
Mélange Zone Central	24.80	94.40	7.93	Priority 1
Moreh (Southern MOC)	24.25	94.28	7.44	Priority 2
Churachandpur Fringe	24.38	93.68	6.46	Priority 3

3.3.3 Fracture stability and hydraulic sensitivity: explicitly assumed scenarios

For the N55°E SHmax scenario at 2.5 km, a deterministic orientation sweep yields a minimum critical pore pressure of 28.49 MPa (margin +3.49 MPa in relation to the assumed 25 MPa initial pressure) at strike 25° and dip 90°. This is a numerical property of an idealized stress tensor and plane grid only. It does not constrain the actual orientations of MOC faults, nor does it demonstrates active hydrogen migration. The full orientation dependence is shown in Figure 12. A rigorous geologic application requires observed fault attitudes, site-specific stress depth profiles and pore pressures. A WSM-informed N25.17°E azimuth alternative leads to a full-grid minimum ΔPcrit of 3.49 MPa (rounded). An example N20°E-striking, 60°-dipping plane needs 10.28 MPa versus 9.12 MPa for the N55°E baseline. Both calculations retain assumed stress magnitudes of 80/65/45 MPa and are not predictions for any mapped MOC fault. The pressure-driven transmissivity gain for the assumed closure law is strongly dependent on baseline effective normal stress (Figure 13). These curves offer relative fluid-access scenarios and cannot be used to claim validated permeability values or increased in-situ serpentinisation flux. Effects of shear dilation, mineral sealing, fracture network connectivity and water supply are not modeled.

3.3.4 Ranking sensitivity and limits of inference

Across the ±20% independently perturbed and renormalized weighting scenarios, the MOC HPI has a 5th–95th percentile interval of 8.343–8.436, conditional on fixed scores. This quantifies internal weight stability, not

absolute geological accuracy. For aggregate-score uncertainty scenarios, the probabilities that each sub-area ranks first are model-dependent and should not be interpreted as measured likelihood of commercial hydrogen (Fig. 14).

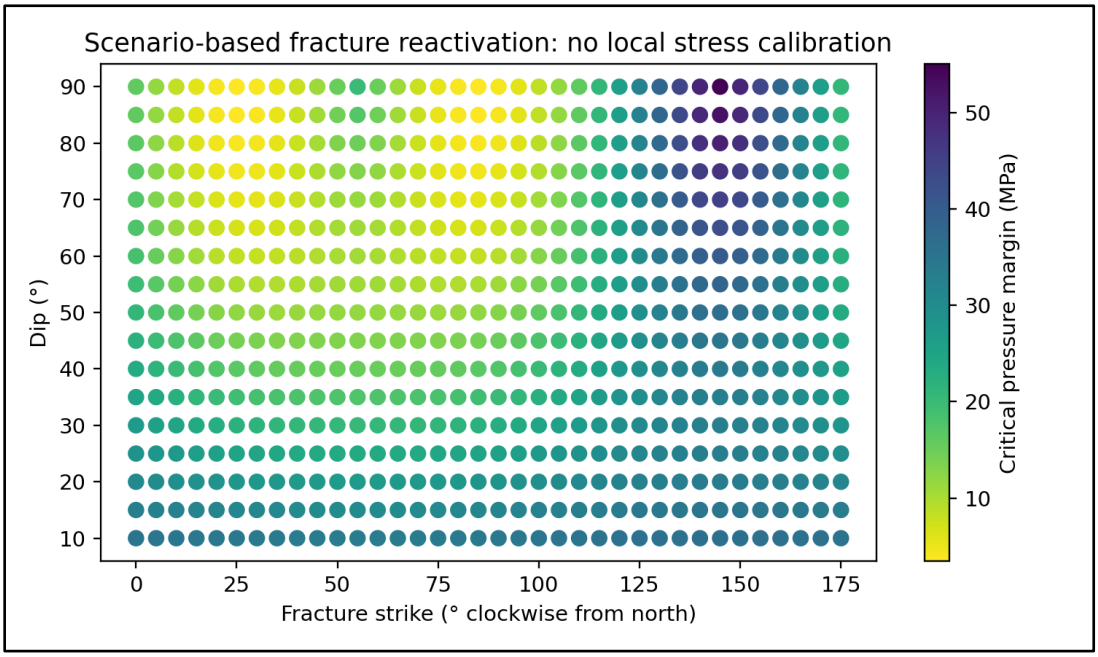


Figure 12. Critical pore-pressure margin across synthetic fracture orientations under a non-calibrated N55°E SHmax stress scenario.

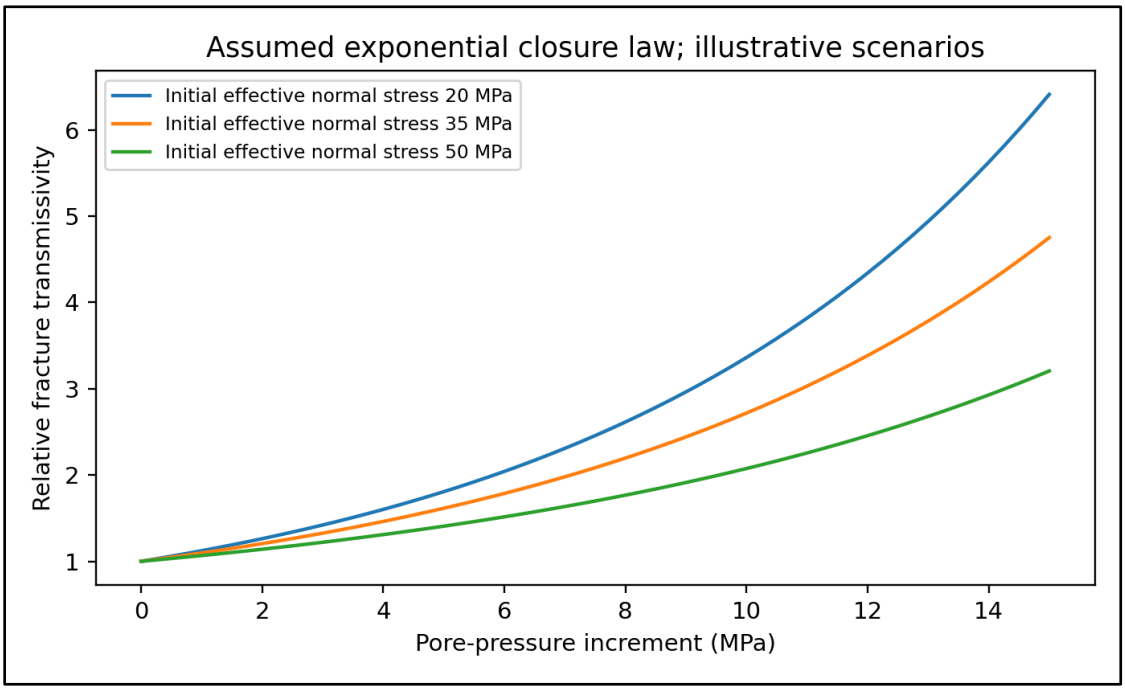


Figure 13. Relative transmissivity under an assumed normal-stress closure law; not field-calibrated permeability.

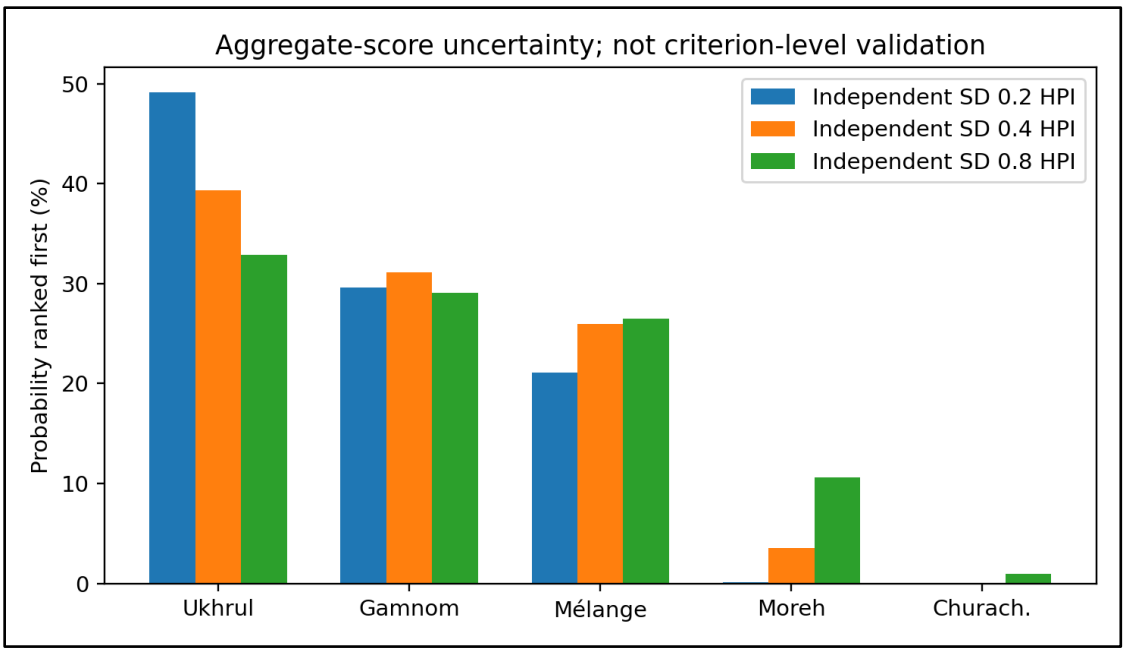


Figure 14. Probability of ranking first under independently perturbed aggregate scores (illustrative uncertainty only).

3.4 Volumetric natural hydrogen resource estimate

Figure 15 shows the five-stage volumetric estimate of H_2 resource in MOC. This estimate is sensitive to assumed effective yield, ultramafic fraction, ophiolite thickness and recovery factor.

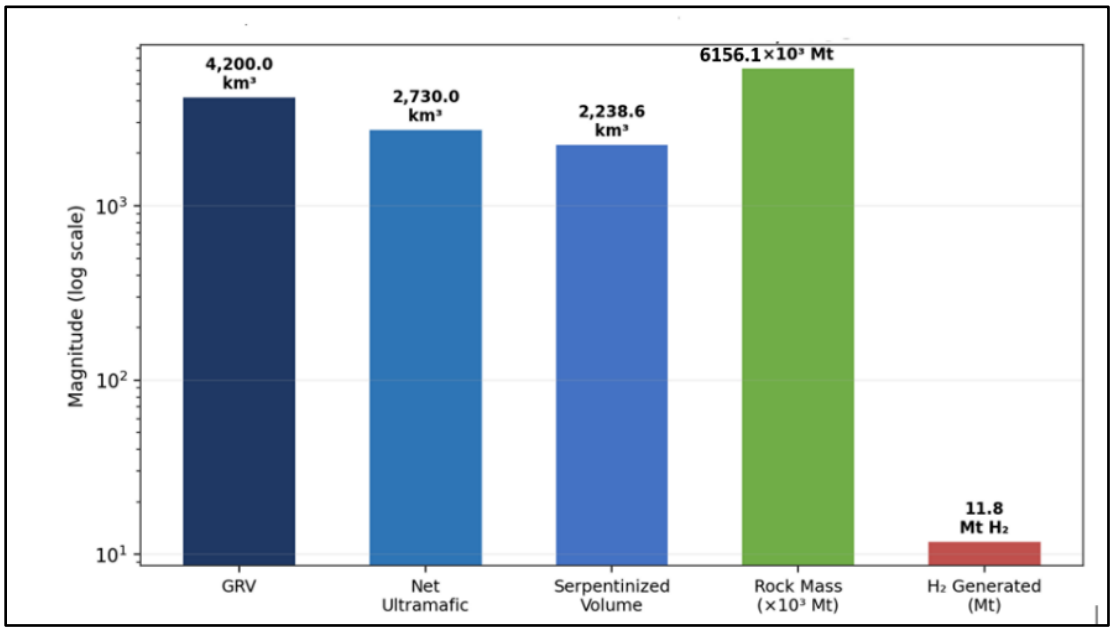


Figure 15. Five-stage volumetric H_2 resource cascade for the MOC (logarithmic scale). Gross rock volume is progressively reduced through ultramafic fraction, serpentinisation degree and stoichiometric yield to ~11.8 Mt of generated H_2.

Table 9. Five-stage volumetric H_2 resource estimate for the MOC.

Stage	Parameter	Value	Unit
1	Ophiolite areal extent	1,200	km^2
1	Average thickness	3.5	km
1	Gross rock volume (GRV)	4,200	km^3
2	Ultramafic fraction	65	%
2	Net ultramafic volume	2,730	km^3
3	Serpentinisation degree	82	%
3	Effective serpentinised volume	2,239	km^3
4	H_2 yield per tonne	0.95	mol/t
4	Total H_2 generated	11.78	Mt H_2
5	Recovery factor (conservative / optimistic)	1.5 / 5.0	%
5	Recoverable H_2 (conservative)	0.18	Mt H_2
5	Recoverable H_2 (optimistic)	0.59	Mt H_2

3.4.2 Sensitivity analysis

The volumetric estimate brings significant uncertainty. A tornado sensitivity analysis (Figure 16) ranks the input parameters by their impact on the H_2 resource. Recovery factor and per-tonne H_2 yield lead the uncertainty, followed by ophiolite area and thickness. Serpentinisation degree and ultramafic fraction exercise reasonably modest leverage because they are already well constrained by the geochemical data. This recognizes recovery-factor characterisation and direct yield measurement as the highest-value targets for initial exploration.

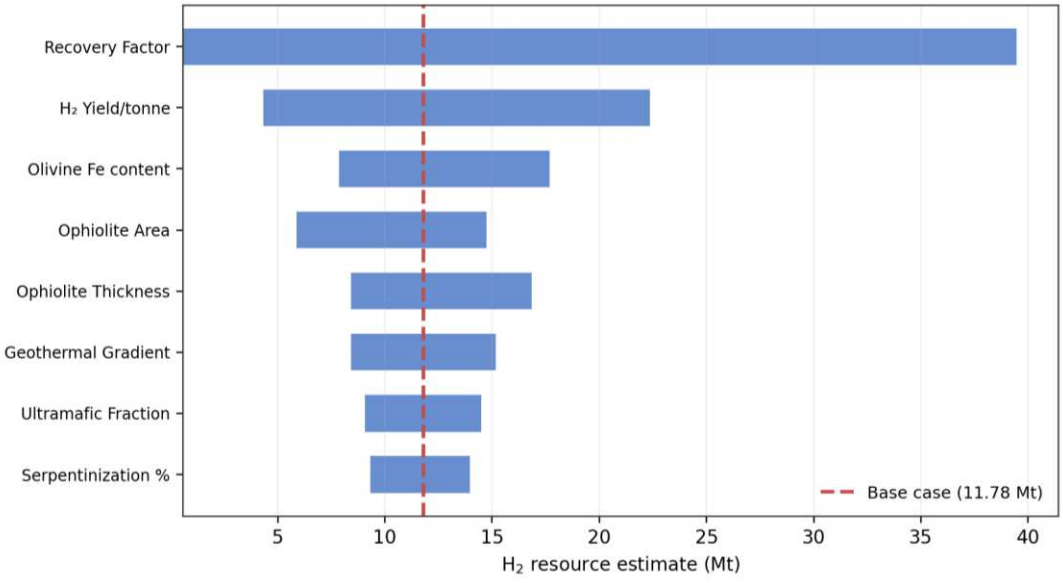


Figure 16. Tornado sensitivity analysis of the MOC H_2 resource estimate. Bars show the resource range as each parameter varies between its P10 and P90 values; the dashed red line is the base case (11.78 Mt). Recovery factor and per-tonne H_2 yield dominate the uncertainty.

3.5 Structural Controls on H_2 Migration

H_2 migration from deep serpentinisation zones to the surface necessitates structural conduits. The MOC sits within one of India's most seismically active zones. The Indo-Burma Range records multiple Mw ≥ 5.0

earthquake annually, with major past events including the 1988 Myanmar border earthquake (Ms 7.3) and the 2016 Manipur earthquake (Mw 6.7). Active reverse and thrust fault systems divide the ophiolite belt. These fault systems create structural permeability analogous to that observed in fault-controlled H_2 migration in the Samail (Oman) and Zambales (Philippines) ophiolites. At outcrop scale, striations and slickenside surfaces in MOC serpentinites indicate recurrent reactivation of shear zones. This generates the fracture permeability that facilitates ongoing serpentinisation and delivers pathways for upward H_2 migration. These conditions also mirror the fault-controlled seep geometry at the Chimaera gas seep, Turkey (7–11 L/s H_2 flux; Etiope, 2023). (Angelier and Baruah 2009). (Kayal et al. 2006).

Within the geomechanical framework of the area, the dominant structures of the MOC are critically stressed. The Churachandpur–Mao Fault, the Kopili Fault Zone, the proximal Sagaing Fault, the IMR Schuppen thrust belt, and the ophiolite mélange zone all preserve fracture apertures conducive to fluid circulation under the present transpressional stress field. The mélange zone is a sheared mixture of serpentinised ultramafic blocks in a talc–chlorite schist matrix. It is globally recognised as an H_2 highway. The prior serpentinisation records past reaction, while the intensely fractured matrix bears present-day permeability.

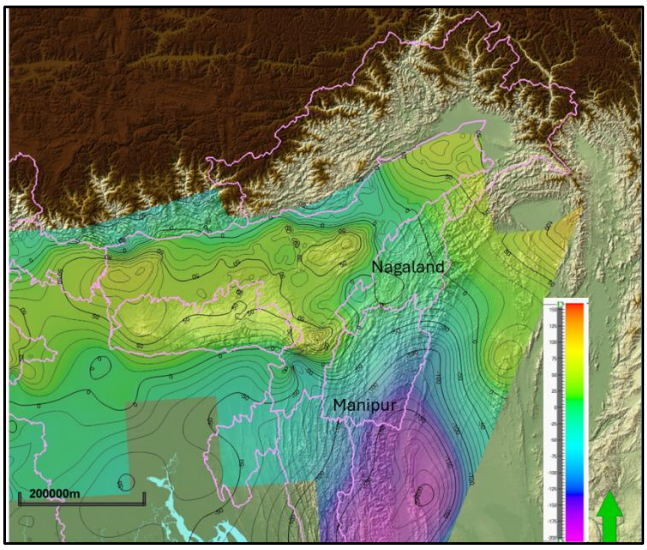


Figure 17. Gravity Residual Map of the area. Data Source: Bureau Gravimétrique International (BGI) / IAG International Gravity Field Service.

The residual-gravity and magnetic-anomaly map (Figure 17) provide complementary geophysical support for natural hydrogen prospectivity in the Manipur–Nagaland ophiolite belt. Strong residual-gravity gradients show noticeable density contrasts related with dense mafic–ultramafic bodies and major crustal discontinuities, whereas the bulging magnetic anomaly corridor through Nagaland and eastern Manipur is compatible with magnetite-bearing ultramafic rocks and variable serpentinisation. Because oxidation of Fe^{2+} during serpentinisation produces magnetite together with H_2, coincidence of magnetic anomalies, gravity gradients, mapped ultramafic rocks and regional faults provides a reasonable source–reaction–migration framework, with faults enabling water access and subsequent H_2 migration (Figure 18). Thus, eastern Manipur and adjoining Nagaland constitute priority targets for natural hydrogen exploration, although the magnetic anomalies alone are not diagnostic of active serpentinisation (Ningthoujam et al. 2012).

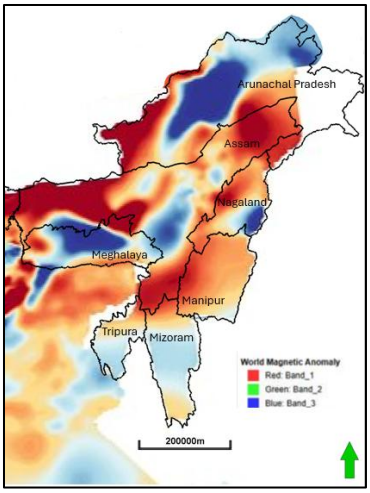


Figure 18. World magnetic anomaly map highlighting the Indo–Burma Range. The map shows the regional magnetic anomaly pattern across the Indo–Burma Range and adjoining tectonic domains, providing a geophysical context for interpreting crustal structure, lithological contrasts and major tectonic boundaries.

3.6 Global Ophiolite Analogues: Benchmark Comparison (Vacquand et al. 2018). (Yao et al. 2025).

The MOC is considered part of the same Neo-Tethyan ophiolite family as several established or well-constrained H_2-productive systems. The Bulqizë (Albania) system is the most instructive direct analogue of this where H_2 concentrations exceeding 50 vol % have been reported in chromitite-rich ophiolitic rocks (Truche et al. 2024). It implicates the combination of serpentinised peridotite and podiform chromitite. This combination is confirmed in the MOC. The Nidar ophiolite (Ladakh) is a direct plate-tectonic correlate of the MOC within the Indus–Tsangpo Suture Zone. It preserves fluid inclusions supporting methane and hydrogen generated during serpentinisation (Sachan et al. 2007). Figure 19 represents the ranks of the key global analogues by their resemblance to the MOC and validation status.

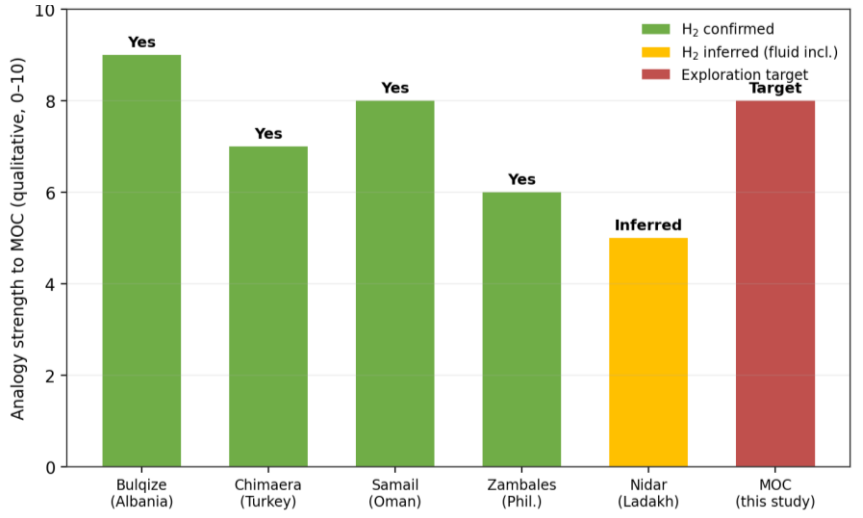


Figure 19. Global ophiolite-hosted H_2 analogues benchmarked against the MOC. Green bars denote systems with confirmed H_2 (Bulqize, Chimaera, Samail, Zambales); amber denotes H_2 inferred from fluid inclusions (Nidar); red marks the MOC as the exploration target. Bar height is the qualitative analogy strength to the MOC.

Table 10. Comparison of the MOC with globally confirmed natural hydrogen-producing ophiolite systems.

Ophiolite / setting	H_2 concentration	Key mechanism	Confirmed	Analogy to MOC
Samail, Oman	Up to 2.5 mL/min seeps	Low-T serpentinisation	Yes	High (SSZ + abyssal)
Bulqizë, Albania	>50 vol % (mine gas)	Serpentinisation + chromitite	Yes	Very high (chromitite-rich)
Zambales, Philippines	0.06–1.20 mg/L dissolved	Serpentinisation + faults	Yes	High (Neo-Tethyan SSZ)
Chimaera, Turkey	7–11 L/s seep	Deep peridotite serpent.	Yes	Moderate (geometry)
Nidar, Ladakh	Fluid inclusions (CH_4+H_2)	Subduction serpent.	Inferred	Very high (direct correlate)
Manipur (MOC)	Not yet measured	Serpentinisation (pervasive)	Target	This study

3.7 National-scale prospectivity ranking framework

3.7.1 Rationale and national context

India's subsurface hosts an excellent variety of geological settings capable of generating molecular hydrogen (H_2). However, its natural hydrogen endowment remains mostly uncharacterised. A preliminary academic estimate places India's in-place natural hydrogen resource at about 3,475 million tonnes, distributed across ophiolite complexes, greenstone belts, cratonic basins, basaltic provinces, and geothermal systems. In contrast to a national hydrogen demand anticipated to rise from ~6 Mt yr^{-1} in 2020 to over 50 Mt yr^{-1} by 2070, and a net-zero target of 2070, this represents a strategically important but unranked opportunity. The Geological Survey of India's confirmation of natural H_2 in the South Andaman ophiolite in February 2025 is India's first such discovery which provides direct validation that the country's ophiolite belts are prospective. It motivates a methodical, evidence-based ranking of candidate zones to guide exploration prioritisation.

A multi-criteria ranking of twenty-one natural hydrogen prospective zones spanning all major Indian generation mechanisms is presented here. Each zone is scored against twelve weighted geological, structural and exploration criteria. The resulting composite Hydrogen Prospectivity Index is used to allocate each zone to one of four prospectivity tiers. The framework is standardized against confirmed H_2-producing systems worldwide and is designed to be updated as field gas-survey and drilling data become accessible.

3.7.2 Overall prospectivity ranking

The ranking of all twenty-one zones obtained after applying the weighted scoring framework is shown in Figure 20. Composite HPI values range from 8.39 for the MOC of the Indo-Burma Range down to 3.94 for the Gondwana–Damodar coalfields. A clear structure appears from the ranking. The five highest-ranked zones are either all ophiolite- or spreading-centre-hosted serpentinisation systems. These are separated by a distinct gap from the broad cluster of geothermal, cratonic, basinal and basaltic zones in the 4.5–5.9 range. The metamorphic and biogenic systems rank lowest. These 21 zones were identified based on evidence-based inclusion criteria that required a plausible hydrogen generation mechanism, supporting geological evidence and sufficient published data for quantitative scoring, thus the ranking should be considered representative, not exhaustive.

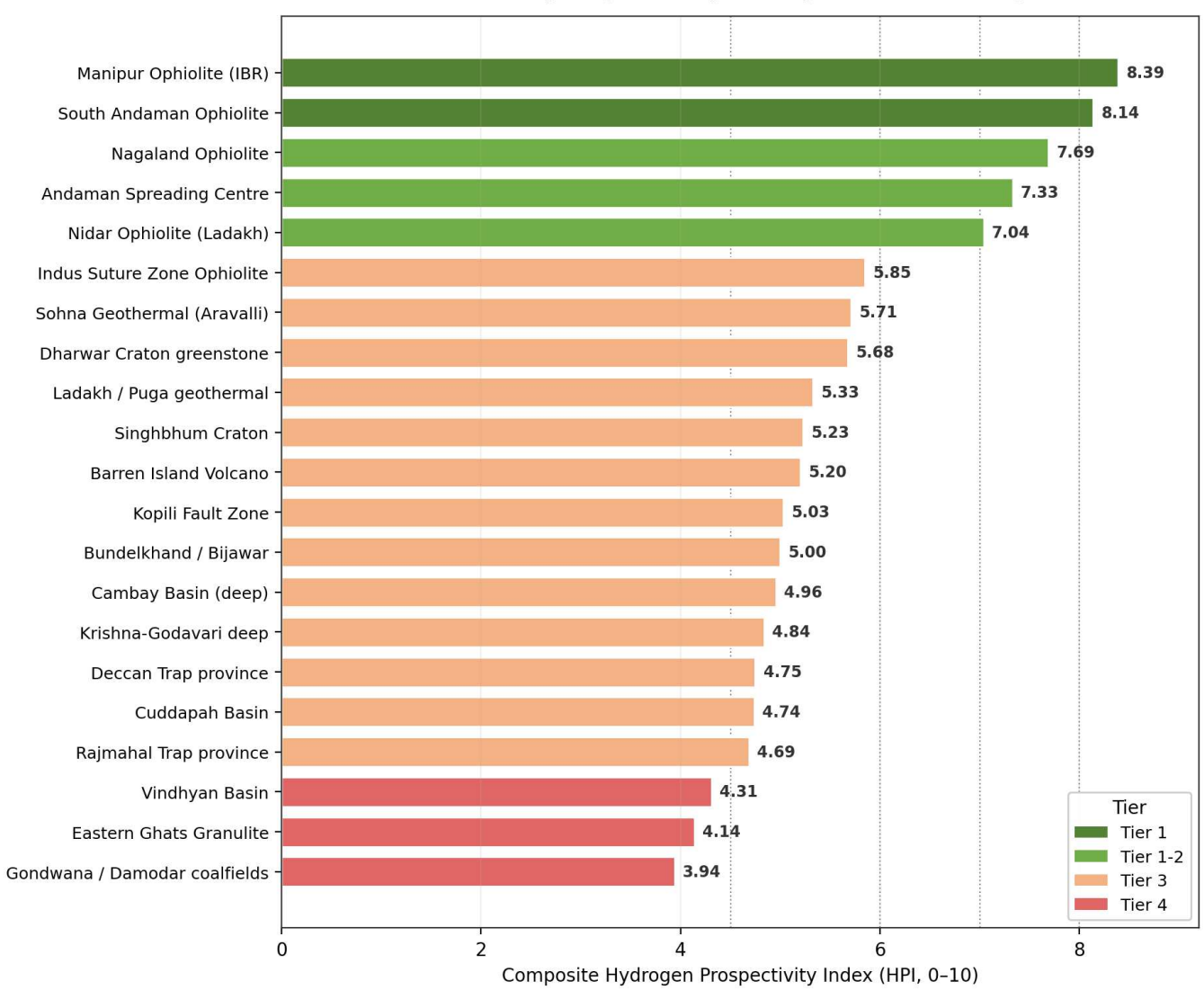


Figure 20. Ranked composite Hydrogen Prospectivity Index for the twenty-one Indian natural hydrogen zones, coloured by tier. Ophiolite-hosted serpentinisation systems (Manipur, South Andaman, Nagaland, Nidar) and the Andaman spreading centre occupy the top tiers; dotted lines mark the tier thresholds.

The MOC ranks first (HPI 8.39), combining maximal source-rock and serpentinisation scores with active transpressional tectonics and a robust global analogue match. The South Andaman ophiolite ranks a close second (8.14), individually advancing from a perfect confirmation score following the 2025 GSI discovery. However, Andaman is offset by its offshore accessibility penalty. The Nagaland ophiolite (7.69), Andaman spreading centre (7.33) and Nidar ophiolite of Ladakh (7.04) are among the other zones within a high-priority group. The distribution of all representative zones is provided in **Figure 21**. The ranking reflects the adopted weighting framework and may change as direct field measurements become available.

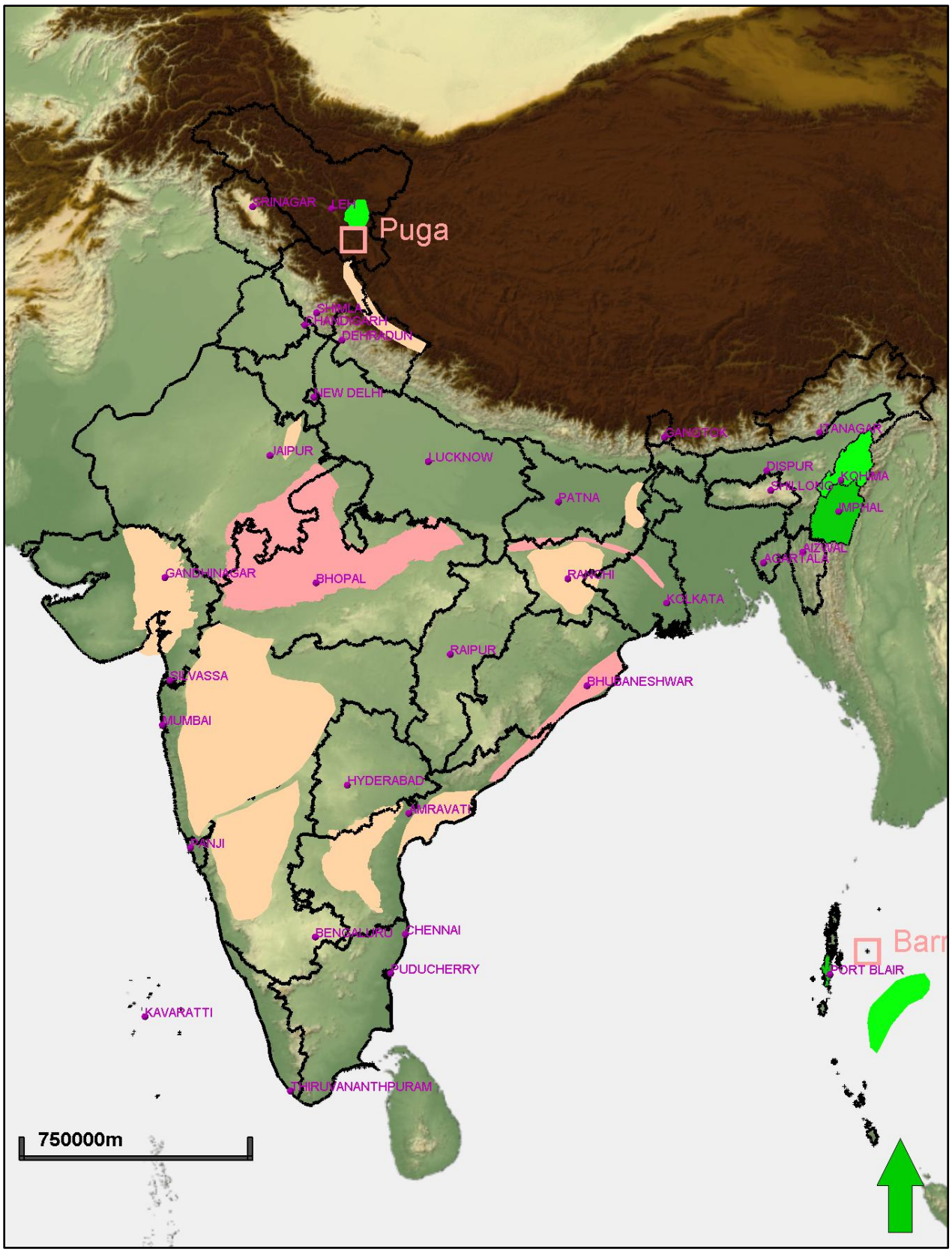


Figure 21. Hydrogen-prospective zones based on multi-criteria ranking.

3.7.3 Tier classification

Zones were clustered into four tiers by composite HPI: Tier 1 (≥ 8.0, prime targets), Tier 1–2 (7.0–7.9, high priority), Tier 3 (4.5–5.9, moderate), and Tier 4 (< 4.5, frontier/low). Figure 22 represents the resultant distribution. Two zones reach Tier 1 and three fall in the Tier 1–2 band, together constituting the five priority targets. The large Tier 3 population reflects the many geologically probable but less favourable craton, basin, basalt and geothermal settings (Figure 22). The top-ranked zones are listed in Table 11.

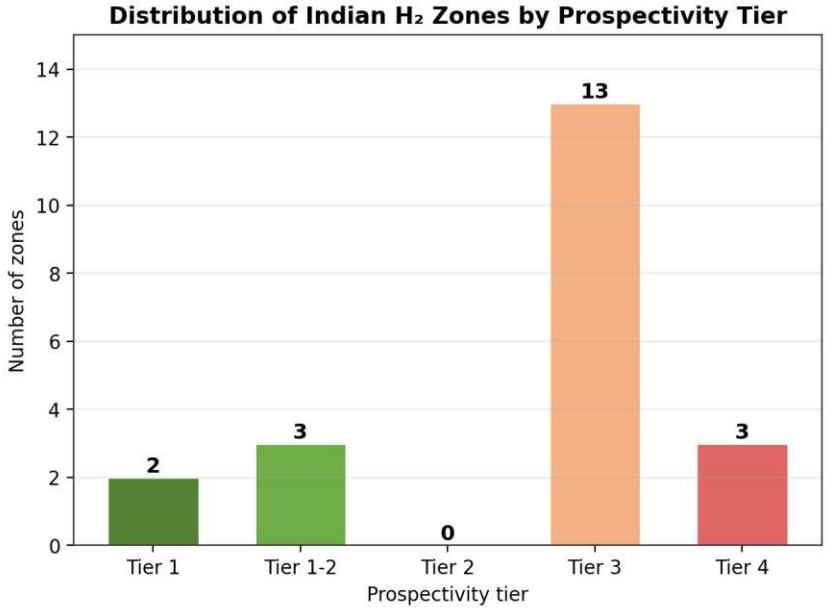


Figure 22. Distribution of the twenty-one Indian H_2 zones across the four prospectivity tiers. The five Tier 1 and Tier-1–2 zones constitute the priority exploration targets.

Table 11. Tier classification of the top-ranked Indian natural hydrogen zones with composite HPI and exploration priority.

Rank	Zone	HPI	Tier	Priority
1	Manipur Ophiolite (IBR)	8.39	Tier 1	Priority 1
2	South Andaman Ophiolite	8.14	Tier 1	Priority 1
3	Nagaland Ophiolite (Naga Hills)	7.69	Tier 1-2	Priority 1
4	Andaman Spreading Centre	7.33	Tier 1-2	Priority 1
5	Nidar Ophiolite (Ladakh)	7.04	Tier 1-2	Priority 1
6	Indus Suture Zone Ophiolite	5.85	Tier 3	Priority 3
7	Sohna Geothermal (Aravalli)	5.71	Tier 3	Priority 3
8	Dharwar Craton greenstone	5.68	Tier 3	Priority 3

3.7.4 Criterion contribution to the composite score

Decomposition of the composite HPI into its weighted criterion contributions is presented in Figure 23. It clarifies why the leading zones rank as they do. For the ophiolite systems, source-rock quality and serpentinisation potential lead the score reflecting their extensively serpentinised harzburgite–dunite protoliths. The South Andaman zone derives a large contribution from the confirmation condition (C8) owing

to the GSI discovery. However, the geothermal (Sohna) and cratonic (Dharwar) zones draw comparably more of their lower totals from fluid availability and logistical accessibility rather than source superiority.

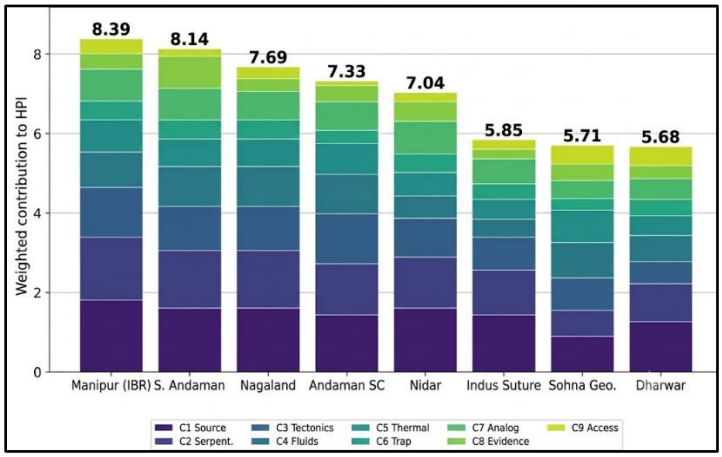


Figure 23. Weighted criterion contributions to the composite HPI for the eight highest-ranked zones. Source-rock quality (C1) and serpentinisation potential (C2) dominate the leading ophiolite scores; the confirmation criterion (C8) is decisive for South Andaman.

3.7.5 Top-five zones: twelve-criterion profiles

The radar profiles of the five priority zones are presented in Figure 24. They reveal their complementary strengths and the criteria that limit each. The Manipur complex achieves near-maximal scores across source, serpentinisation, tectonics and analogue axes. However, it is limited only by trap definition and the absence of direct field confirmation. South Andaman is the most balanced profile and the only one reaching the maximum on the evidence axis although South Andaman is penalised on accessibility. The Andaman spreading centre scores highest on tectonics and thermal regime but lowest on accessibility, while Nidar is limited by its arid, fluid-limited setting.

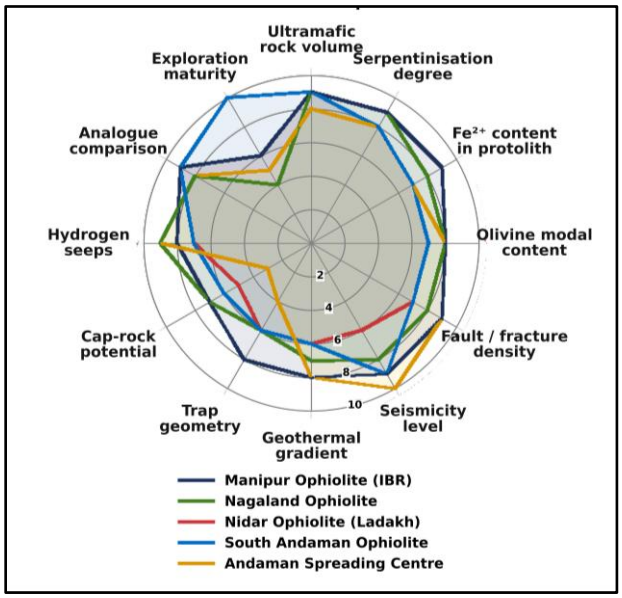


Figure 24. Twelve-criterion radar profiles of the top-five Indian H_2 zones. Each axis is scored 0–10.

3.8 National mechanism and analogue perspective

3.8.1 Mechanism-based national prospectivity

Applying the rating scheme of Section 2.5.1 to the Indian geological inventory yields the national mechanism ranking of Table 12. Two mechanisms are rated ★★★★★: continental serpentinisation in the Indo-Burma Range ophiolites and forearc serpentinisation in the Andaman-Nicobar province, the latter now supported by the 2025 GSI confirmation of natural H_2. A cluster of ★★★ mechanisms, deep-slab dehydration, radiolysis, and thermogenic cracking, defines a secondary tier distributed across the Indo-Burma subduction root, the Singhbhum Craton, and the Cambay Basin respectively. The remaining mechanisms are rated ★★ or ★, being either volumetrically limited, structurally dispersed, or subject to rapid consumption.

Table 12. Classification of natural hydrogen generation mechanisms, optimal settings, best Indian locations, and prospectivity ratings. The rating scheme is defined in Section 2.5.1.

#	Mechanism	Core reaction / process (balanced)	Best Indian location	Rating	Key reference(s)
1	Serpentinisation (continental)	3 Fe_2SiO_4 + 2 H_2O → 2 Fe_3O_4 + 3 SiO_2 + 2 H_2 (fayalite component; forsterite hydration forms serpentine + brucite without H_2)	Indo-Burma Range: MOC (Ukhrul, Tengnoupal–Moreh), Naga Hills	★★★★★	Klein et al. 2013; Zgonnik 2020; MOC data (this study)
2	Serpentinisation (forearc/marine)	Seawater-driven fayalite oxidation as (1); water supplied to forearc peridotite during subduction/obduction	Andaman–Nicobar Ophiolite Province	★★★★★	DGH 2025; Zgonnik 2020
3	Deep-slab dehydration	Serpentine → forsterite + talc/enstatite + H_2O at depth; released fluids drive further peridotite serpentinisation (reaction 1)	Indo-Burma subduction root (Manipur–Nagaland)	★★★	Zgonnik 2020
4	Radiolysis of water	2 H_2O →(α,β,γ from U,Th,^{40}K) 2 H_2 + O_2	Singhbhum Craton deep boreholes (Jharkhand)	★★★	Lin et al. (2005a); Lin et al. (2005b); Sherwood Lollar et al. 2014
5	Thermogenic cracking	Kerogen → CH_4 + higher hydrocarbons + H_2 + C(residue) at >150 °C, R_o > 2 %	Cambay Basin deep wells (Gujarat)	★★★	Tissot & Welte 1984; Zgonnik 2020
6	Mechanochemical (seismic)	≡Si–O–Si≡ + fracture → ≡Si–O• + •Si≡; ≡Si• + H_2O → ≡Si–OH + ½ H_2 (surface radicals react with water)	Kopili Fault Zone (Assam); MCT (Himalaya)	★★	Kita et al. 1982; Hirose et al. 2011
7	Metamorphic dehydration	Hydrous silicate → anhydrous phase + H_2O; partial reduction of released H_2O by Fe^{2+} → H_2	Eastern Ghats Granulite Belt (Odisha–AP)	★★	Zgonnik 2020
8	Mantle / volcanic degassing	Primary H_2 (and H_2 from magmatic H_2O + Fe^{2+} melt equilibria) exsolved during degassing	Barren Island Volcano (Andaman Sea)	★★	Zgonnik 2020; Sherwood Lollar et al. 2014
9	Low-T iron oxidation	3 FeO + H_2O → Fe_3O_4 + H_2 (Fe^{2+} in basalt/BIF/komatiite + meteoric water)	Dharwar Craton greenstone belts (Karnataka)	★	Mayhew et al. 2013; Zgonnik 2020
10	Biogenic (subsurface)	Organic matter → CO_2 + H_2 (fermentation); rapidly consumed by H_2-oxidising microbes	Damodar Valley coalfields (Jharkhand–WB)	★	Hallenbeck & Benemann 2002; Zgonnik 2020

3.8.2 Global analogue calibration

The analogue-match criterion (C11) was calibrated against ten globally important natural hydrogen systems (Figure 25). The Bourakebougou field (Mali) and the Bulqizë ophiolite (Albania) represent two of the most significant global benchmarks (Table 13). The latter, which produces >50 vol.% H_2 from chromitite-bearing serpentinite, serves as the principal analogue for India's chromitite-rich ophiolite belts and underpins the highest analogue scores assigned in this study. The Samail ophiolite (Oman), Chimaera seep system (Turkey), Zambales ophiolite (Philippines), and New Caledonia serpentinisation systems provide strong analogues for the Indo-Burma Range and Andaman ophiolites. The Indian occurrences at Nidar and South Andaman now form part of the emerging global natural hydrogen evidence base.

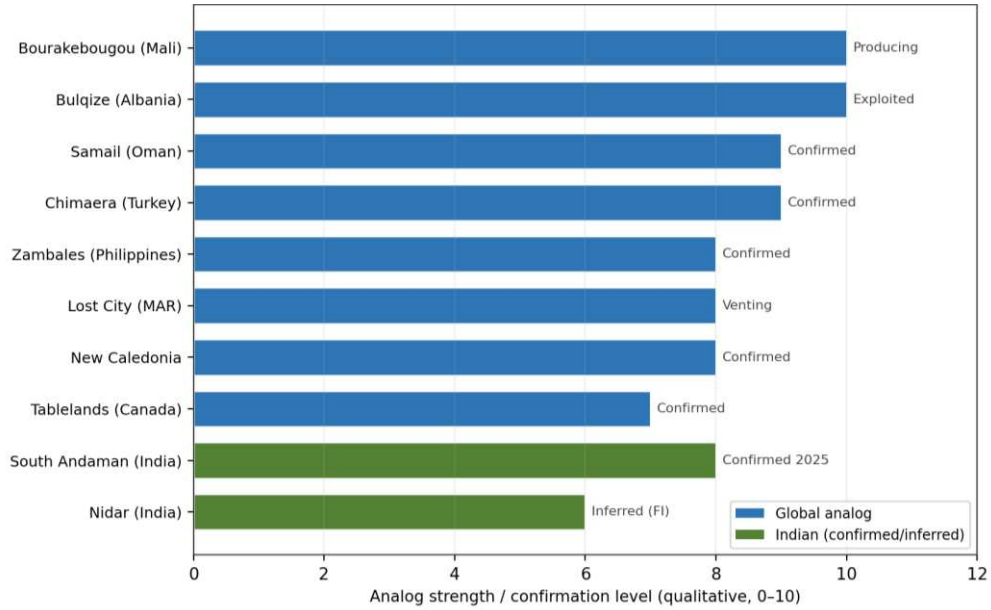


Figure 25. Global natural hydrogen analogue systems used to calibrate the analogue-match criterion. Indian occurrences (green) at South Andaman (confirmed 2025) and Nidar (fluid-inclusion evidence) are shown alongside the international benchmarks.

Table 13. Global analogue systems, their hydrogen signatures, and the closest Indian counterparts.

Analogue system	H_2 signature	Mechanism	Closest Indian zone
Bourakebougou, Mali	98 % H_2; 5–8 t/day	Cratonic Fe-oxidation	Singhbhum / Dharwar cratons
Bulqizë, Albania	>50 vol % (mine gas)	Serpentinisation + chromitite	Manipur (chromitite-rich)
Samail, Oman	Up to 12 mmol/L springs	Low-T serpentinisation	Manipur / Nagaland
Chimaera, Turkey	7–11 L/s seep	Deep peridotite serpent.	Manipur (structural)
Zambales, Philippines	0.06–1.20 mg/L	Serpentinisation + faults	Manipur / Andaman
South Andaman, India	Detected (DGH 2025)	Forearc serpentinisation	(Indian discovery)
Nidar, India	Fluid inclusions (CH_4+H_2)	Subduction serpent.	(Indian inferred)

4. Discussion

4.1 Geomechanics as the differentiator among Indian provinces

Such a comparative analysis of Indian provinces provides a compelling illustration that geomechanical conditions are the main factor that differentiates H_2 prospectivity in superficially similar geochemistry of ophiolites. Though the Singhbhum and Dharwar ultramafic rocks have lithologies similar to the IBR (olivine-bearing), the stable craton settings result in fracture networks being long-healed, effective stresses being high, and fluid circulation being minimal. They are fossil serpentinites, geochemically complete but volumetrically inert. Conversely, the MOC is characterised by a critically stressed fault network, maintained by active Indo-Asian convergence, episodic co-seismic permeability enhancement, suture-zone overpressure and exothermic reaction-induced fracturing, which together form a geomechanically renewable H_2 generation system. If unmodified olivine remains and water passes through then both will be satisfied in the IBR for H_2 generation.

4.2 H_2 generation potential and economic context

Serpentinised peridotites contain 0.1–16.2 mL H_2 kg^{-1} rock, far exceeding any other ophiolitic lithology (Etiope, 2024), and the serpentinites of the MOC are the volumetrically dominant unit across a belt extending for hundreds of kilometres. For economic context, the Bourakebougou field (Mali) produces 58 t H_2/day at an estimated ~US$ 1/kg which is far below green hydrogen (US$ 3-6/kg in 2024 Europe) and blue hydrogen (US$ 1.5-2.5/kg). The Manipur region with existing road infrastructure and proximity to the growing energy markets of Northeast India is well positioned for a phased exploration programme.

4.3 Trapping, preservation and microbial consumption

The MOC system is associated with two major risks. First, trapping: serpentinite itself is an inadequate seal because of its ductile behaviour, but the interbedded pelagic sediments (radiolarian cherts, mudstones) and the ophiolite-flysch contact are candidate stratigraphic seals that have to be characterised in detail. The role of serpentinisation-formed magnetite in the preservation of H_2 is also complex (Geymond et al. 2023). Second, microbial consumption: hydrogenotrophic methanogens and sulphate-reducers are able to consume significant portions of generated H_2, as documented in the Samail shallow aquifers. However, the fault-controlled delivery of H_2 to the surface in the seismically active, rapidly exhuming MOC is also plausible and can escape microbial oxidation. This favours fault-controlled escape over diffuse microbially consumed seepage. (Neuzil 1994).

4.4 India's strategic opportunity

India's H_2 strategy today is almost solely focused on green (electrolytic) and blue (CCS-coupled) pathways. With a domestic ophiolite belt with confirmed serpentinite sequences and with GSI already confirming natural H_2 in the Andaman ophiolite (2025), there is a strong scientific and strategic case for India to pioneer geological H_2 exploration in South Asia. Localized geologic H_2 production in Northeast India could support hydrogen fuel-cell transport, industrial feedstock for regional fertilizer plants, and grid balancing, aligning the MOC opportunity with the NGHM and broader Northeast-India development agenda.

4.5 Implications for National Exploration Prioritisation

The ranking carries three key suggestions for Indian natural hydrogen exploration. First, the dominance of ophiolite-hosted serpentinisation at the top of the ranking, combined with the established South Andaman

discovery supports concentration of early-stage onshore exploration on the Indo-Burma Range, specifically the Manipur and Nagaland ophiolite belts. The highest source and reaction scores coincide with accessible continental exposure of this area. Second, the Andaman ophiolite and spreading-centre systems, although offshore, warrant continued exploration given the existing GSI confirmation and the active hydrothermal regime. Third, the Tier 3 cratonic and geothermal zones including Dharwar, Singhbhum, Bundelkhand and the Sohna and Ladakh geothermal fields represent a second wave of targets that are onshore and accessible. These locations also benefit from analogue calibration to the Mali cratonic and geothermal systems.

The framework is purposely transparent and scalable because each composite score is a simple weighted sum of documented criterion scores, the ranking can be refined as new evidence such as soil-gas H_2 flux surveys, spring geochemistry, magnetotelluric imaging, and exploratory drilling becomes available for any zone. The confirmation criterion is anticipated to rise sharply for zones where direct H_2 is detected. The scores presented here reflect expert-judgement calibration against the presently published geological, geochemical and structural evidence and against established global analogues. They are intended as a defensible starting point for national exploration planning rather than a final assessment.

In summary, the multi-criteria ranking recognizes the MOC and the South Andaman ophiolite as India's Tier 1 natural hydrogen targets. The Nagaland ophiolite, Andaman spreading centre and Nidar ophiolite form a high-priority Tier 1–2 group. These five serpentinisation-hosted systems should anchor a phased national exploration programme associated with the National Green Hydrogen Mission and India's 2070 net-zero objective.

4.6 Limitations and uncertainties

This first-pass desktop assessment uses published and analogue data only; no H_2 measurements or MOC-specific subsurface data are available. The estimated 11.8 Mt generated H_2 and 0.18–0.59 Mt recoverable H_2 are therefore order-of-magnitude scenarios, not regulatory resources. Major uncertainties arise from sparse heterogeneous geochemical data, unknown subsurface extent and thickness, assumed serpentinisation, yield and recovery factors, inferred stress and pore-pressure conditions, and unverified reservoir–seal integrity; actual recoverability may approach zero. The corrected energy equivalent is 0.021–0.071 EJ. Prospectivity scores are comparative and dependent on expert weighting, and all conclusions require validation through soil-gas, spring-gas, geophysical and drilling data. The volumetric estimate should be considered an order-of-magnitude exploration-screening calculation. Future work should employ Monte Carlo uncertainty propagation as direct subsurface and hydrogen-flow data become available.

4.7 Recommended Exploration Roadmap

Building on the geomechanical framework and the prospectivity ranking, a five-phase, progressively intensive exploration programme is proposed. Table 14 summarises the phases, methods, decision gates and priority sectors.

Table 14. Phased natural hydrogen exploration roadmap for the MOC.

Phase	Timeline	Key activity	Output	Priority areas
1	Year 1	Literature synthesis & remote sensing (Sentinel-2, ALOS-PALSAR, ASTER)	Serpentinite & lineament maps	Ukhrul–Nungbi; Gamnom

Phase	Timeline	Key activity	Output	Priority areas
2	Year 1–2	Soil-gas & spring geochemistry (H_2, CH_4, He; δD, $\delta^{13}C$)	Surface H_2/CH_4/He anomalies	Mélange zone; Moreh
3	Year 2–3	Geophysics: gravity, magnetics, magnetotellurics, seismic	Subsurface structure; trap geometry	All Priority 1 sectors
4	Year 3–4	Exploration drilling (2–3 slim holes, 500–1,500 m)	In-situ H_2 concentration; flow rates	Best 2 targets
5	Year 4–5	Appraisal: isotopic analysis; production testing	Resource volume; commerciality	Proven sector

5. Conclusions

This integrated geological, geochemical, structural, geomechanical and volumetric assessment of natural hydrogen prospectivity for the MOC, set within a pan-Indian mechanism framework, is the first of its kind. The principal conclusions are as follows.

- Of the ten crustal H_2 generation mechanisms operating across India (Table 12, Section 3.8), serpentinisation of ophiolitic harzburgite and dunite is the dominant viable pathway, and the Indo-Burma Range hosts its optimal expression. The MOC emerges as one of India's most prospective ophiolite-hosted natural hydrogen targets within the adopted framework, combining Tier 1 ultramafic protolith, active transpressional tectonics, abundant meteoric fluid supply, and an optimal thermal window at accessible subsurface depth.
- Geomechanical conditions may affect fluid access and migration, but are not established as the dominant prospectivity control. Fracture networks associated with Indo-Burma convergence and reaction-induced fracturing may influence permeability controlling reactant delivery and H_2 migration, subject to unverified local hydraulic connectivity.
- Whole-rock geochemistry (MgO 35.2–44.21 wt %, Cr 1200–4572 ppm, Ni 1800–4138 ppm, TiO_2 0.01–0.10 wt %), Cr-spinel chemistry (Cr# 0.47–0.83), Nd-isotope systematics, and the incidence of népouite together indicate a depleted, fluid-altered, olivine-rich substrate favourable for serpentinisation-driven H_2 generation. The MOC chromitite compositions overlap those of the H_2-producing Bulqizë ophiolite (Truche et al. 2024; Touré et al. 2026).
- A serpentinisation phase-equilibria model places the MOC geotherm within the optimal H_2 generation window at mid-crustal depth. A twelve-criterion prospectivity assessment places the complex in the Excellent tier, with a weighted composite score of 8.39 out of 10. Intra-belt scoring identifies the Ukhrul–Nungbi sector (8.1), Gamnom–Shangshak (8.0), and the central mélange zone (7.9) as Priority 1 targets for H_2 exploration.
- A conservative five-stage volumetric model, adopting an effective yield of 0.95 mol H_2 per tonne and 82 % serpentinisation, estimates a screening-level generated resource of 11.8 Mt of H_2 within the MOC, with a recoverable range of 0.18–0.59 Mt and an energy equivalent of roughly 0.02–0.07 EJ under present recovery assumptions. The estimate requires validation through direct H_2

measurements. Sensitivity analysis identifies the recovery factor and per-tonne yield as the dominant uncertainties and therefore the highest-value early exploration targets within the adopted framework.

- These figures are a first-pass, order-of-magnitude assessment built from published data and analogue reasoning, not a validated resource estimate. The principal uncertainties, chief among them the absence of any direct H_2 measurement in the complex and the unconstrained recovery factor, are set out in Section 4.6 and define the priorities for the next phase of work.
- A phased exploration roadmap comprising remote sensing, soil-gas and spring geochemistry, geophysics, exploratory drilling, and appraisal is recommended. The MOC represents one of the most promising exploration targets identified in this study yet uncharted natural hydrogen targets in South and Southeast Asia, and its systematic exploration is a high-priority scientific and strategic objective aligned with India's National Green Hydrogen Mission.

Acknowledgements

The authors are thankful to Indian Institute of Technology (Indian School of Mines) Dhanbad-826004, India for facilitating the research.

Statements and Declarations

Author contributions

Dilip Kumar Mahata.: Conceptualization, Methodology, Investigation, Formal analysis, Data curation, Visualization, Writing - original draft, Writing – review and editing.

Sayantan Ghosh: Validation, Resources, Supervision, Writing – review and editing.

Competing interests: The authors declare that they have no relevant financial or non-financial interests to disclose.

Funding: The authors received no specific external funding for this work.

Declaration of generative AI and AI-assisted technologies

During the preparation of this work, the authors used Claude, developed by Anthropic, to assist with plotting of data, language refinement, organisation, and readability. After using this tool, the authors reviewed, verified, and edited the content as necessary and take full responsibility for the content of the published article.

Data availability: The compiled criterion scores, adopted stress and fracture assumptions, WSM 2025 regional extract, synthetic fault-plane calculations, transmissivity sensitivities, Monte Carlo inputs and volumetric checks are supplied in the companion workbook Manipur_Hydrogen_Traceable_Calculations_WSM2025.xlsx, provided as Supplementary Dataset S1. The underlying World Stress Map Database Release 2025 is publicly accessible at https://doi.org/10.5880/WSM.2025.001. Original published geochemical measurements remain attributed to their cited source studies. No new field measurements of MOC hydrogen concentrations were acquired.

References

Abrajano TA, Sturchio NC, Bohlke JK, Lyon GL, Poreda RJ, Stevens CM (1988) Methane-hydrogen gas seeps, Zambales Ophiolite, Philippines: Deep or shallow origin? Chem Geol. 71(1-3):211-22. https://doi.org/10.1016/0009-2541(88)90116-7

Acharyya SK (1986) Tectono-stratigraphic history of Naga Hills Ophiolites. Mem Geol Surv India. 119:94-103.

Acharyya SK (2007) Collisional emplacement history of the Naga-Andaman ophiolites and the position of the eastern Indian suture. J Asian Earth Sci. 29(2-3):229-42. https://doi.org/10.1016/j.jseaes.2006.03.003

Acharyya SK (2010) Tectonic evolution of Indo-Burma Range with special reference to Naga-Manipur Hills. In: Ibotombi S, editor. Indo-Myanmar Ranges in the Tectonic Framework of the Himalaya and Southeast Asia. Mem Geol Soc India. 75:25-43.

Alam J, Chatterjee R, Dasgupta S (2019) Estimation of pore pressure, tectonic strain and stress magnitudes in the Upper Assam basin: A tectonically active part of India. Geophys J Int. 216:659-75. https://doi.org/10.1093/gji/ggy440

Andreani M, Mével C, Boullier AM, Escartín J (2007) Dynamic control on serpentine crystallization in veins: Constraints on hydration processes in oceanic peridotites. Geochem Geophys Geosyst. 8(2):Q02012. https://doi.org/10.1029/2006GC001373

Angelier J, Baruah S (2009) Seismotectonics in Northeast India: A stress analysis of focal mechanism solutions of earthquakes and its kinematic implications. Geophys J Int. 178(1):303-26. https://doi.org/10.1111/j.1365-246X.2009.04107.x

Arai S (1994) Characterization of spinel peridotites by olivine-spinel compositional relationships: Review and interpretation. Chem Geol. 113(3–4):191–204. https://doi.org/10.1016/0009-2541(94)90066-3

Ballentine CJ, Karolytė R, Cheng A, Sherwood Lollar B, Gluyas JG, Daly MC (2025) Natural hydrogen resource accumulation in the continental crust. Nat Rev Earth Environ. 6(5):342-56. https://doi.org/10.1038/s43017-025-00670-1

Banerjee P, Bürgmann R, Nagarajan B, Apel E (2008) Intraplate deformation of the Indian subcontinent. Geophys Res Lett. 35(18):L18301. https://doi.org/10.1029/2008GL035468

Barnes I, O'Neil JR, Trescases JJ (1978) Present day serpentinization in New Caledonia, Oman and Yugoslavia. Geochim Cosmochim Acta. 42(1):144-5. https://doi.org/10.1016/0016-7037(78)90225-9

Barton N, Bandis S, Bakhtar K (1985) Strength, deformation and conductivity coupling of rock joints. International Journal of Rock Mechanics and Mining Sciences & Geomechanics Abstracts 22(3):121–140. https://doi.org/10.1016/0148-9062(85)93227-9

Barton CA, Zoback MD, Moos D (1995) Fluid flow along potentially active faults in crystalline rock. Geology 23(8):683–686. https://doi.org/10.1130/0091-7613(1995)023<0683:FFAPAF>2.3.CO;2

Bendall B (2022) Current perspectives on natural hydrogen: a synopsis. MESA Journal 96:37–46. Department for Energy and Mining, South Australia.

Blay-Roger R, Bach W, Bobadilla LF, Ramirez Reina T, Odriozola JA, Amils R, et al (2024) Natural hydrogen in the energy transition: Fundamentals, promise, and enigmas. Renew Sustain Energy Rev. 189:113888. https://doi.org/10.1016/j.rser.2023.113888

Boruah A, Mitra P, Saad KA, Phukan A (2025) Exploring natural hydrogen in India: Screening criteria and prospect evaluation. Improved Oil Gas Recovery. 9. https://doi.org/10.14800/IOGR.1433

Byerlee J (1978) Friction of rocks. Pure Appl Geophys. 116:615-26. https://doi.org/10.1007/BF00876528

Chaubey M, Singh AK, Singh BP, Imtisunep S, Dutt A, Satyanarayanan M, et al (2022) Refertilization of depleted mantle peridotite in the Nagaland–Manipur ophiolite, north-east India: Constraints from PGE, mineral, and whole-rock geochemistry. Geol J. 57(12):5265–5283. https://doi.org/10.1002/gj.4411

Coveney RM Jr, Goebel ED, Zeller EJ, Dreschhoff GAM, Angino EE (1987) Serpentinization and the origin of hydrogen gas in Kansas. AAPG Bull. 71(1):39-48. https://doi.org/10.1306/94886D3F-1704-11D7-8645000102C1865D

Deschamps F, Godard M, Guillot S, Hattori K (2013) Geochemistry of subduction zone serpentinites: A review. Lithos. 178:96-127. https://doi.org/10.1016/j.lithos.2013.05.019

Devi LD, Singh NI (2011) Geochemical study of peridotites from the Manipur Ophiolite Complex, Northeast India with special reference to their PGE concentration. J Geol Soc India. 77(3):273-9. https://doi.org/10.1007/s12594-011-0035-2

Dey A, Hussain MF, Barman MN (2018) Geochemical characteristics of mafic and ultramafic rocks from the Naga Hills Ophiolite, India: Implications for petrogenesis. Geosci Front. 9(2):517-29. https://doi.org/10.1016/j.gsf.2017.05.006

Dick HJB, Bullen T (1984) Chromian spinel as a petrogenetic indicator in abyssal and alpine-type peridotites and spatially associated lavas. Contrib Mineral Petrol. 86(1):54–76. https://doi.org/10.1007/BF00373711

Directorate General of Hydrocarbons (2025) India's Hydrocarbon Outlook 2024–2025. Directorate General of Hydrocarbons, Ministry of Petroleum and Natural Gas, Government of India, New Delhi, Sect. 9.5.3, Natural Hydrogen Initiative.

Dutta AJ, Gogoi N, Hussain FZ, Kulkarni SD (2024) Integrated coupled assessment of geostorage and geothermal prospects in the oil fields of Upper Assam Basin. Sci Rep. 14(1):12390. https://doi.org/10.1038/s41598-024-60292-3

Ellis GS, Gelman SE (2024) Model predictions of global geologic hydrogen resources. Sci Adv. 10(50):eado0955. https://doi.org/10.1126/sciadv.ado0955

Emmanuel S, Berkowitz B (2006) Suppression and stimulation of seafloor hydrothermal convection by exothermic mineral hydration. Earth Planet Sci Lett. 243(3-4):657-68. https://doi.org/10.1016/j.epsl.2006.01.028

Etiope G, Sherwood Lollar B (2013) Abiotic methane on Earth. Rev Geophys. 51(2):276-99. https://doi.org/10.1002/rog.20011

Etiope G (2023) Massive release of natural hydrogen from a geological seep (Chimaera, Turkey): Gas advection as a proxy of subsurface gas migration and pressurised accumulations. Int J Hydrogen Energy. 48(25):9172-84. https://doi.org/10.1016/j.ijhydene.2022.12.025

Etiope G (2024) Natural hydrogen extracted from ophiolitic rocks: A first dataset. Int J Hydrogen Energy. 78:368-72. https://doi.org/10.1016/j.ijhydene.2024.06.292

Evans P (1964) The tectonic framework of Assam. J Geol Soc India. 5(1):80-96. https://doi.org/10.17491/jgsi/1964/050111

Evans BW (2004) The serpentinite multisystem revisited: Chrysotile is metastable. Int Geol Rev. 46(6):479-506. https://doi.org/10.2747/0020-6814.46.6.479

Evans BW (2008) Control of the products of serpentinization by the $Fe^{2+}Mg^{-1}$ exchange potential of olivine and orthopyroxene. J Petrol. 49(10):1873-87. https://doi.org/10.1093/petrology/egn050

Fareeduddin, Dilek Y (2015) Structure and petrology of the Nagaland-Manipur Hill Ophiolitic Mélange Zone, NE India: A fossil Tethyan subduction channel at the India-Burma plate boundary. Episodes. 38(4):298-314. https://doi.org/10.18814/epiiugs/2015/v38i4/82426

Frost BR (1985) On the stability of sulfides, oxides, and native metals in serpentinite. J Petrol. 26(1):31-63. https://doi.org/10.1093/petrology/26.1.31

Frost BR, Beard JS (2007) On silica activity and serpentinization. J Petrol. 48(7):1351-68. https://doi.org/10.1093/petrology/egm021

Fryer P, Wheat CG, Mottl MJ (1999) Mariana blueschist mud volcanism: Implications for conditions within the subduction zone. Geology 27(2):103–106. https://doi.org/10.1130/0091-7613(1999)027<0103:MBMVIF>2.3.CO;2

Gahalaut VK, Kundu B, Laishram SS, Catherine J, Kumar A, Singh MD, et al (2013) Aseismic plate boundary in the Indo-Burmese wedge, northwest Sunda Arc. Geology. 41(2):235-8. https://doi.org/10.1130/G33771.1

Geymond U, Briolet T, Combaudon V, Sissmann O, Martinez I, Duttine M, et al (2023) Reassessing the role of magnetite during natural hydrogen generation. Front Earth Sci. 11:1169356. https://doi.org/10.3389/feart.2023.1169356

Ghose NC, Chatterjee N, Fareeduddin (2014) Geology of the Naga Hills Ophiolite. In: Ghose NC, Chatterjee N, Fareeduddin. A Petrographic Atlas of Ophiolite: An example from the eastern India-Asia collision zone. New Delhi: Springer. p. 25-48. https://doi.org/10.1007/978-81-322-1569-1_3

Ghosh B, Ray J, Morishita T (2014) Grain-scale plastic deformation of chromite from podiform chromitite of the Naga-Manipur ophiolite belt, India: Implication to mantle dynamics. Ore Geol Rev. 56:199-208. https://doi.org/10.1016/j.oregeorev.2013.09.001

Hacker BR (2008) H_2O subduction beyond arcs. Geochem Geophys Geosyst. 9(3):Q03001. https://doi.org/10.1029/2007GC001707

Heidbach O, Rajabi M, Cui X, Fuchs K, Müller B, Reinecker J, et al (2016) The World Stress Map database release. : Crustal stress pattern across scales. Tectonophysics. 2018;744:484-98. https://doi.org/10.1016/j.tecto.2018.07.007

Heidbach O, Rajabi M, Di Giacomo D, Harris J, Lammers S, Morawietz S, Pierdominici S, Reiter K, von Specht S, Storchak D, Ziegler MO (2025) World Stress Map Database Release 2025. GFZ Data Services. https://doi.org/10.5880/WSM.2025.001

Hirose T, Kawagucci S, Suzuki K (2011) Mechanoradical H_2 generation during simulated faulting: Implications for an earthquake-driven subsurface biosphere. Geophys Res Lett. 38:L17303. https://doi.org/10.1029/2011GL048850

Holland G, Sherwood Lollar B, Li L, Lacrampe-Couloume G, Slater GF, Ballentine CJ (2013) Deep fracture fluids isolated in the crust since the Precambrian era. Nature. 497(7449):357-60. https://doi.org/10.1038/nature12127

Hubbert MK, Rubey WW (1959) Role of fluid pressure in mechanics of overthrust faulting. Geological Society of America Bulletin 70(2):115–166. https://doi.org/10.1130/0016-7606(1959)70[115:ROFPIM]2.0.CO;2

Ingebritsen SE, Sanford WE, Neuzil CE (2006) Groundwater in geologic processes. 2nd ed. Cambridge: Cambridge University Press. https://doi.org/10.1017/9780511807855

International Energy Agency (IEA) (2025) Global hydrogen review. Paris: IEA; 2025.

Jamtveit B, Malthe-Sørenssen A, Kostenko O (2008) Reaction enhanced permeability during retrogressive metamorphism. Earth Planet Sci Lett. 267(3-4):620-7. https://doi.org/10.1016/j.epsl.2007.12.016

Kamenetsky VS, Crawford AJ, Meffre S (2001) Factors controlling chemistry of magmatic spinel: An empirical study of associated olivine, Cr-spinel and melt inclusions from primitive rocks. J Petrol. 42(4):655–671. https://doi.org/10.1093/petrology/42.4.655.

Kayal JR, Arefiev SS, Barua S, Hazarika D, Gogoi N, Kumar A, et al (2006) Shillong plateau earthquakes in northeast India region: Complex tectonic model. Curr Sci. 91(1):109-14.

Kelemen PB, Matter J, Streit EE, Rudge JF, Curry WB, Blusztajn J (2011) Rates and mechanisms of mineral carbonation in peridotite: Natural processes and recipes for enhanced, in situ CO_2 capture and storage. Annu Rev Earth Planet Sci. 39:545-76. https://doi.org/10.1146/annurev-earth-092010-152509

Kelemen PB, Hirth G (2012) Reaction-driven cracking during retrograde metamorphism: Olivine hydration and carbonation. Earth Planet Sci Lett. 345-348:81-9. https://doi.org/10.1016/j.epsl.2012.06.018

Kelley DS, Karson JA, Früh-Green GL, Yoerger DR, Shank TM, Butterfield DA, et al (2005) A serpentinite-hosted ecosystem: The Lost City hydrothermal field. Science. 307(5714):1428-34. https://doi.org/10.1126/science.1102556

Kesari GK (2011) Geology and mineral resources of Manipur, Mizoram, Nagaland and Tripura. Geological Survey of India, Miscellaneous Publication No. 30, Part IV, Vol 1 (Part 2), Shillong, India.

Khogenkumar S, Singh AK, Singh RKB, Khanna PP, Singh NI, Singh WI (2016) Coexistence of MORB and OIB-type mafic volcanics in the Manipur Ophiolite Complex, Indo-Myanmar Orogenic Belt, northeast India: Implication for heterogeneous mantle source at the spreading zone. J Asian Earth Sci. 116:42-58. https://doi.org/10.1016/j.jseaes.2015.11.007

King GCP, Stein RS, Lin J (1994) Static stress changes and the triggering of earthquakes. Bull Seismol Soc Am. 84(3):935–953. https://doi.org/10.1785/BSSA0840030935

Kingson O, Bhutani R, Dash JK, Sebastian S, Balakrishnan S (2017) Resolving the conundrum in origin of the Manipur Ophiolite Complex, Indo-Myanmar range: Constraints from Nd isotopic ratios and elemental concentrations in serpentinized peridotite. Chem Geol. 460:117-29. https://doi.org/10.1016/j.chemgeo.2017.04.021

Kita I, Matsuo S, Wakita H (1982) H_2 generation by reaction between H_2O and crushed rock: An experimental study on H_2 degassing from the active fault zone. J Geophys Res. 87(B13):10789-95. https://doi.org/10.1029/JB087iB13p10789

Klein F, Bach W, McCollom TM (2013) Compositional controls on hydrogen generation during serpentinization of ultramafic rocks. Lithos. 178:55–69. https://doi.org/10.1016/j.lithos.2013.03.008

Kundu B, Gahalaut VK (2013) Tectonic geodesy revealing geodynamic complexity of the Indo-Burmese arc region, North East India. Curr Sci. 104(7):920-33.

Lamzamuan G, Devi SK, Gogoi L (2024) Unraveling the protolith origin of serpentinite rocks from the Tengnoupal area, Manipur Ophiolite Complex, Indo-Myanmar Range. Indian Journal of Science and Technology 17(36):3719–3732. https://doi.org/10.17485/ijst/v17i36.2279

Lefeuvre N, Truche L, Donzé F-V, Ducoux M, Barré G, Fakoury R-A, et al (2021) Native H_2 exploration in the western Pyrenean foothills. Geochem Geophys Geosyst. 22(8):e2021GC009917. https://doi.org/10.1029/2021GC009917

Lin LH, Hall J, Lippmann-Pipke J, Ward JA, Sherwood Lollar B, DeFlaun M, et al (2005) Radiolytic H_2 in continental crust: Nuclear power for deep subsurface microbial communities. Geochem Geophys Geosyst. 6(7):Q07003. https://doi.org/10.1029/2004GC000907

Lin LH, Slater GF, Sherwood Lollar B, Lacrampe-Couloume G, Onstott TC (2005) The yield and isotopic composition of radiolytic H_2, a potential energy source for the deep subsurface biosphere. Geochim Cosmochim Acta. 69(4):893-903. https://doi.org/10.1016/j.gca.2004.07.032

Mahadevan TM (2002) Geology of Bihar and Jharkhand. Geological Society of India, Bangalore, 563 pp.

Maiga O, Deville E, Laval J, Prinzhofer A, Diallo AB (2023) Characterization of the spontaneously recharging natural hydrogen reservoirs of Bourakebougou in Mali. Sci Rep. 13:11876. https://doi.org/10.1038/s41598-023-38977-y

Martin B, Fyfe WS (1970) Some experimental and theoretical observations on the kinetics of hydration reactions with particular reference to serpentinization. Chem Geol. 6(3):185-202. https://doi.org/10.1016/0009-2541(70)90018-5

McCollom TM, Bach W (2009) Thermodynamic constraints on hydrogen generation during serpentinization of ultramafic rocks. Geochim Cosmochim Acta. 73(3):856-75. https://doi.org/10.1016/j.gca.2008.10.032

McCollom TM (2013) Laboratory simulations of abiotic hydrocarbon formation in Earth's deep subsurface. Rev Mineral Geochem. 75:467-94. https://doi.org/10.2138/rmg.2013.75.15

McCollom TM (2016) Abiotic methane formation during experimental serpentinization of olivine. Proc Natl Acad Sci U S A. 113(49):13965-70. https://doi.org/10.1073/pnas.1611843113

Merdith AS, Daniel I, Sverjensky D, Andreani M, Mather B, Williams S, et al (2023) Global hydrogen production during high-pressure serpentinization of subducting slabs. Geochem Geophys Geosyst. 24(10):e2023GC010947. https://doi.org/10.1029/2023GC010947

Milkov AV (2022) Molecular hydrogen in surface and subsurface natural gases: Abundance, origins and ideas for deliberate exploration. Earth Sci Rev. 230:104063. https://doi.org/10.1016/j.earscirev.2022.104063

Mitchell AHG (1993) Cretaceous-Cenozoic tectonic events in the western Myanmar (Burma)-Assam region. J Geol Soc. 150(6):1089-102. https://doi.org/10.1144/gsjgs.150.6.1089

Mottl MJ, Wheat CG, Fryer P, Gharib J, Martin JB (2004) Chemistry of springs across the Mariana forearc shows progressive devolatilization of the subducting plate. Geochim Cosmochim Acta. 68(23):4915-33. https://doi.org/10.1016/j.gca.2004.05.037

Mukhopadhyay D (2001) The Archaean nucleus of Singhbhum: The present state of knowledge. Gondwana Res. 4(3):307-18. https://doi.org/10.1016/S1342-937X(05)70331-2

Naqvi SM (2005) Geology and evolution of the Indian plate: From Hadean to Holocene, 4 Ga to 4 Ka. New Delhi: Capital Publishing Company

Neal C, Stanger G (1983) Hydrogen generation from mantle source rocks in Oman. Earth Planet Sci Lett. 66:315-20. https://doi.org/10.1016/0012-821X(83)90144-9

Neal C, Stanger G (1985) Past and present serpentinisation of ultramafic rocks: an example from the Semail Ophiolite Nappe of Northern Oman. In: Drever JI (ed) The Chemistry of Weathering. NATO ASI Series C, vol 149. Springer, Dordrecht, pp 249–275. https://doi.org/10.1007/978-94-009-5333-8_15

Neuzil CE (1994) How permeable are clays and shales? Water Resour Res. 30(2):145-50. https://doi.org/10.1029/93WR02930

Neuzil CE (2003) Hydromechanical coupling in geologic processes. Hydrogeol J. 11(1):41-83. https://doi.org/10.1007/s10040-002-0230-8

Ningthoujam PS, Dubey CS, Guillot S, Fagion AS, Shukla DP (2012) Origin and serpentinization of ultramafic rocks of Manipur Ophiolite Complex in the Indo-Myanmar subduction zone, Northeast India. J Asian Earth Sci. 50:128-40. https://doi.org/10.1016/j.jseaes.2012.01.004

O'Hanley DS (1996) Serpentinites: Records of tectonic and petrological history. New York: Oxford University Press

Ovung TN, Ray J, Ghosh B, Mandal D, Dasgupta P, Paul M (2017) Occurrence of Népouite in the Serpentinite of the Manipur Ophiolite Belt, Northeastern India: Implication for melt-rock interaction in a supra-subduction zone. J Geol Soc India. 90(2):154-8. https://doi.org/10.1007/s12594-017-0693-9

Pal T, Bhattacharya A, Nagendran G, Yanthan NM, Singh R, Raghumani N (2014) Petrogenesis of chromites from the Manipur ophiolite belt, NE India: Evidence for a supra-subduction zone setting prior to Indo-Myanmar collision. Mineral Petrol. 108(5):713-26. https://doi.org/10.1007/s00710-014-0320-z

Pasquale V, Verdoya M, Chiozzi P (2017) Geothermics: Heat flow in the lithosphere. 2nd ed. Cham: Springer. https://doi.org/10.1007/978-3-319-52084-1

Pearce JA (2014) Immobile element fingerprinting of ophiolites. Elements. 10(2):101–108. https://doi.org/10.2113/gselements.10.2.101

Plümper O, Royne A, Magrasó A, Jamtveit B (2012) The interface-scale mechanism of reaction-induced fracturing during serpentinization. Geology. 40(12):1103-6. https://doi.org/10.1130/G33390.1

Pollack HN, Hurter SJ, Johnson JR (1993) Heat flow from the Earth's interior: analysis of the global data set. Rev Geophys. 31:267–80. https://doi.org/10.1029/93RG01249

Prinzhofer A, Cissé CST, Diallo AB (2018) Discovery of a large accumulation of natural hydrogen in Bourakebougou (Mali). Int J Hydrogen Energy. 43(42):19315-26. https://doi.org/10.1016/j.ijhydene.2018.08.193

Rao RUM, Roy S, Srinivasan R (2003) Heat-flow researches in India: Results and perspectives. In: Mahadevan TM, Arora BR, Gupta KR, editors. Indian Continental Lithosphere: Emerging Research Trends. Mem Geol Soc India. 53:347-91.

Rüpke LH, Morgan JP, Hort M, Connolly JAD (2004) Serpentine and the subduction zone water cycle. Earth Planet Sci Lett. 223(1-2):17-34. https://doi.org/10.1016/j.epsl.2004.04.018

Rutqvist J, Stephansson O (2003) The role of hydromechanical coupling in fractured rock engineering. Hydrogeol J. 11(1):7-40. https://doi.org/10.1007/s10040-002-0241-5

Sachan HK, Mukherjee BK, Bodnar RJ (2007) Preservation of methane generated during serpentinization of upper mantle rocks: Evidence from fluid inclusions in the Nidar ophiolite, Indus Suture Zone, Ladakh (India). Earth Planet Sci Lett. 257(1-2):47-59. https://doi.org/10.1016/j.epsl.2007.02.023

Saha AK (1994) Crustal evolution of Singhbhum-North Orissa, Eastern India. Mem Geol Soc India. 27:1-341.

Schmidt MW, Poli S (1998) Experimentally based water budgets for dehydrating slabs and consequences for arc magma generation. Earth Planet Sci Lett. 163(1-4):361-79. https://doi.org/10.1016/S0012-821X(98)00142-3

Seewald JS (2003) Organic-inorganic interactions in petroleum-producing sedimentary basins. Nature. 426(6964):327-33. https://doi.org/10.1038/nature02132

Sengupta S, Acharyya SK, Van Den Hul HJ, Chattopadhyay B (1989) Geochemistry of volcanic rocks from the Naga Hills Ophiolites, northeast India and their inferred tectonic setting. J Geol Soc. 146(3):491-8. https://doi.org/10.1144/gsjgs.146.3.0491

Sherwood Lollar B, Voglesonger K, Lin LH, Lacrampe-Couloume G, Telling J, Abrajano TA, et al (2007) Hydrogeologic controls on episodic H_2 release from Precambrian fractured rocks—Energy for deep subsurface life on Earth and Mars. Astrobiology. 7(6):971-86. https://doi.org/10.1089/ast.2006.0096

Sherwood Lollar B, Onstott TC, Lacrampe-Couloume G, Ballentine CJ (2014) The contribution of the Precambrian continental lithosphere to global H_2 production. Nature. 516(7531):379-82. https://doi.org/10.1038/nature14017

Sibson RH (1992) Implications of fault-valve behaviour for rupture nucleation and recurrence. Tectonophysics. 211(1-4):283-93. https://doi.org/10.1016/0040-1951(92)90065-E

Sibson RH (1994) Crustal stress, faulting and fluid flow. Geol Soc Lond Spec Publ. 78:69-84. https://doi.org/10.1144/GSL.SP.1994.078.01.07

Singh AK (2008) PGE distribution in the ultramafic rocks and chromitites of the Manipur Ophiolite Complex, Indo-Myanmar Orogenic Belt, Northeast India. J Geol Soc India 72(5):649–660. https://doi.org/10.17491/jgsi/2008/720507

Singh AK (2013) Petrology and geochemistry of abyssal peridotites from the Manipur Ophiolite Complex, Indo-Myanmar Orogenic Belt, Northeast India: Implication for melt generation in mid-oceanic ridge environment. J Asian Earth Sci 66:258–276. https://doi.org/10.1016/j.jseaes.2013.02.004

Singh AK, Ao A (2025) Origin, evolution, and emplacement of the Nagaland-Manipur ophiolites, Indo-Myanmar orogenic belt, Northeast India. Proc Indian Natl Sci Acad 91:672–686. https://doi.org/10.1007/s43538-024-00353-3

Singh AK, Nayak R, Khogenkumar S, Subramanyam KSV, Thakur SS, Singh RKB, Satyanarayanan M (2017) Genesis and tectonic implications of cumulate pyroxenites and tectonite peridotites from the Nagaland–Manipur ophiolites, Northeast India: constraints from mineralogical and geochemical characteristics. Geol J 52(3):415–436. https://doi.org/10.1002/gj.2769

Singh AK, Singh NI, Devi LD, Singh RKB (2012) Geochemistry of mid-ocean ridge mafic intrusives from the Manipur Ophiolitic Complex, Indo-Myanmar Orogenic Belt, NE India. J Geol Soc India 80(2):231–240. https://doi.org/10.1007/s12594-012-0133-9

Singh NI, Devi LD, Chanu TY (2013) Petrological and geochemical study of serpentinised peridotites from the southern part of Manipur Ophiolitic Complex, Northeast India. J Geol Soc India 82(2):121–132. https://doi.org/10.1007/s12594-013-0130-7

Singh TG, Soibam I, Theunuo K, Pal T, Singh CD, Singh MP, Ajit K (2024) High grade garnet clinopyroxene bearing metamorphic sole from south-eastern Manipur Ophiolite Belt. J Geosci Res 9(2):82–94. https://doi.org/10.56153/g19088-023-0188-55

Sleep NH, Meibom A, Fridriksson T, Coleman RG, Bird DK (2004) H_2-rich fluids from serpentinization: Geochemical and biotic implications. Proc Natl Acad Sci U S A. 101(35):12818-23. https://doi.org/10.1073/pnas.0405289101

Soibam I, Singh MP (2006) Analysis of drainage systems of Manipur and implications on the tectonics of the Indo-Myanmar Ranges. In: Saklani PS (ed) Himalaya: Geological Aspects, vol 4. Satish Serial Publishing House, New Delhi, pp 281–302.

Steefel CI, Appelo CAJ, Arora B, Jacques D, Kalbacher T, Kolditz O, et al (2015) Reactive transport codes for subsurface environmental simulation. Comput Geosci. 19(3):445-78. https://doi.org/10.1007/s10596-014-9443-x

Sukumaran PV (2024) Geological hydrogen: A new carbon-free, clean energy vector. J Geol Soc India. 100(3):447-50. https://doi.org/10.17491/jgsi/2024/173852

Sun B, Zhang M, Sun Q, Zhong J, Shao G (2025) Review on natural hydrogen wells safety. Nat Commun. 16:369. https://doi.org/10.1038/s41467-024-55773-y

Szponar N, Brazelton WJ, Schrenk MO, Bower DM, Steele A, Morrill PL (2013) Geochemistry of a continental site of serpentinization, the Tablelands Ophiolite, Gros Morne National Park: A Mars analogue. Icarus. 224(2):286-96. https://doi.org/10.1016/j.icarus.2012.07.004

Telling J, Boyd ES, Bone N, Jones EL, Tranter M, MacFarlane JW, et al (2015) Rock comminution as a source of hydrogen for subglacial ecosystems. Nat Geosci. 8(11):851-5. https://doi.org/10.1038/ngeo2533

Templeton AS, Ellison ET, Kelemen PB, Leong J, Boyd ES, Colman DR, et al (2024) Low-temperature hydrogen production and consumption in partially-hydrated peridotites in Oman: Implications for stimulated geological hydrogen production. Front Geochem. 2:1366268. https://doi.org/10.3389/fgeoc.2024.1366268

Terzaghi K (1943) Theoretical soil mechanics. New York: John Wiley & Sons. https://doi.org/10.1002/9780470172766

Toft PB, Arkani-Hamed J, Haggerty SE (1990) The effects of serpentinization on density and magnetic susceptibility: A petrophysical model. Phys Earth Planet Inter. 65(1-2):137-57. https://doi.org/10.1016/0031-9201(90)90082-9

Touré K, Loisy C, Cerepi A, Goskolli E, Muceku B (2026) Natural hydrogen migration and trapping in the Bulqizë ophiolitic massif (Albania). Fuel. 426:139595. https://doi.org/10.1016/j.fuel.2026.139595

Townend J, Zoback MD (2000) How faulting keeps the crust strong. Geology 28(5):399–402. https://doi.org/10.1130/0091-7613(2000)28<399:HFKTCS>2.0.CO;2

Truche L, McCollom TM, Martinez I (2020) Hydrogen and abiotic hydrocarbons: Molecules that change the world. Elements. 16(1):13-8. https://doi.org/10.2138/gselements.16.1.13

Truche L, Donzé FV, Goskolli E, Muceku B, Loisy C, Monnin C, et al (2024) A deep reservoir for hydrogen drives intense degassing in the Bulqizë ophiolite. Science. 383(6683):618-21. https://doi.org/10.1126/science.adk9099

Ulmer P, Trommsdorff V (1995) Serpentine stability to mantle depths and subduction-related magmatism. Science. 268(5212):858-61. https://doi.org/10.1126/science.268.5212.858

Vacquand C, Deville E, Beaumont V, Guyot F, Sissmann O, Pillot D, et al (2018) Reduced gas seepages in ophiolitic complexes: Evidences for multiple origins of the H_2-CH_4-N_2 gas mixtures. Geochim Cosmochim Acta. 223:437-61. https://doi.org/10.1016/j.gca.2017.12.018

Valdiya KS (2016) The making of India: Geodynamic evolution. 2nd ed. Cham: Springer. https://doi.org/10.1007/978-3-319-25029-8

van Keken PE, Hacker BR, Syracuse EM, Abers GA (2011) Subduction factory: 4. Depth-dependent flux of H_2O from subducting slabs worldwide. J Geophys Res Solid Earth. 116:B01401. https://doi.org/10.1029/2010JB007922

Vidyadharan KT, Joshi A, Ghosh S, Gaur MP, Shukla R (1989) Manipur Ophiolites: Its geology, tectonic setting and metallogeny. In: Ghose NC, editor. Phanerozoic Ophiolites of India. Patna: Sumna Publications. p. 197-212.

Warr O, Young ED, Giunta T, Kohl IE, Ash JL, Sherwood Lollar B (2021) High-resolution, long-term isotopic and isotopologue variation identifies the sources and sinks of methane in a deep subsurface carbon cycle. Geochim Cosmochim Acta. 294:315–34. https://doi.org/10.1016/j.gca.2020.12.002

Wegner WW, Ernst WG (1983) Experimentally determined hydration and dehydration reaction rates in the system MgO-SiO_2-H_2O. Am J Sci. 283-A:151-80.

Yao Y, Donzé FV, Persem M, Truche L, Muceku B, Garambois S, et al (2025) Magnetotellurics point to serpentinization as a potential source of hydrogen in the Bulqizë Ophiolite. J Geophys Res Solid Earth. 130(10):e2025JB031898. https://doi.org/10.1029/2025JB031898

Zgonnik V (2020) The occurrence and geoscience of natural hydrogen: A comprehensive review. Earth Sci Rev. 203:103140. https://doi.org/10.1016/j.earscirev.2020.103140

Zoback MD (2007) Reservoir geomechanics. Cambridge: Cambridge University Press. https://doi.org/10.1017/CBO9780511586477

Zoback MD, Gorelick SM (2012) Earthquake triggering and large-scale geologic storage of carbon dioxide. Proc Natl Acad Sci U S A. 109(26):10164-8. https://doi.org/10.1073/pnas.1202473109

Supplementary Files

This is a list of supplementary files associated with this preprint. Click to download.

- ManipurHydrogenTraceableCalculationsWSM2025.xlsx